Deep Resources Engineering 2 (2025) 100197

Contents lists available at ScienceDirect

Deep Resources Engineering

journal homepage: www.keaipublishing.com/en/journals/deepre/

Simulation of progressive notch failure in deep bored raises using an iterative approach in FLAC3D

Alex Hall [a,b,*], Ming Cai [b,c], Chris O'Connor [d], Pranay Yadav [a], Brad Simser [a]

[a] Glencore Sudbury Integrated Nickel Operations, Sudbury, Canada
[b] School of Engineering and Computer Science, Laurentian University, Sudbury, Canada
[c] MIRARCO – Mining Innovation, Laurentian University, Sudbury, Canada
[d] VALE, Sudbury, Canada

ARTICLE INFO

Keywords:
Bored raise
Vertical excavations
Notching
Stress fracturing
Scouring
Numerical simulation

ABSTRACT

The study examines empirical and numerical modeling methods that can be used to predict the depth of notch failure in bored raises excavated for Glencore's Onaping Depth project within the Craig Mine complex in Sudbury, Ontario, Canada, at depths between 1150 and 1915 m. These raises experienced significant notch growth throughout their entire length. A detailed assessment found four mechanisms of deterioration causing the notch growth. Of these mechanisms, stress fracturing and scouring contributed to most of the notch growth. These two mechanisms, when working together, magnify their individual effects, making their combined contributions difficult to predict using existing empirical approaches and numerical models. Hence, a new and innovative approach is presented to simulate the progressive notch failure observed in the Onaping Depth raises using FLAC3D. Due to the inability of FLAC3D to simulate rock fracturing directly, an iterative process is established where elements that meet a damage criterion considering cohesion and volumetric strain are removed from the model, and the model equilibrium is restabilized with additional damage forming. The final stabilized notches simulated with FLAC3D show a good agreement with the geometry observed in the raises. This representation of notch failure is more realistic, which is different from the conventional approach of using yielded elements to represent failure zones in continuum models. This work provides insight into deterioration in bored raises and establishes a framework for predicting deterioration and its growth, thereby enhancing the understanding of rock mass response to mining activities.

1. Introduction

As mines progress deeper and new orebodies exceed the efficient range of existing infrastructure, internal vertical shaft (winze) excavations become the fastest and the most economical means of accessing deep ore deposits [36]. Most often, a network of vertical infrastructure is required to support lateral development and bulk mining activities. In general, there are multiple vertical excavations between levels for ventilation, material movement, and egress, in addition to a large-diameter shaft equipped with a hoisting system that brings the necessary materials to depth and hoists the waste and ore rocks to the surface. These excavations can be completed by mechanical raiseboring or by more labor-intensive methods such as sinking/slashing and Alimak mining.

In the last 20 years, there has been a significant shift in the mining industry to limit operator exposure and, if possible, remove operators from the mining face. Therefore, mechanically cut bored raises have become more widespread in use due to the ability to remove operators from the advancing excavation.

These vertical excavations are high cost in relation with lateral development excavations because of economies of scale, with lateral development outweighing vertical development by several orders of magnitude. This makes the equipment, and the expertise used in vertical excavations more specialized than in lateral development. It also makes data collection and proactive engineering highly important for these critical excavations.

Unlike the drill-and-blast excavation method, where the rock mass is supported after each blast, bored raises are excavated continuously, often over long distances, and could remain unsupported for extended durations or indefinitely. In strong brittle rocks at shallow to

* Corresponding author at: Glencore Sudbury Integrated Nickel Operations, Sudbury, Canada.
E-mail address: alex.hall@glencore.ca (A. Hall).

https://doi.org/10.1016/j.deepre.2025.100197
Received 24 March 2025; Received in revised form 13 May 2025; Accepted 15 May 2025
Available online 18 May 2025

intermediate depths, where no stress-driven rock mass failure occurs, bored raises do not need to be supported. However, at increasing depths where mining-induced wall stresses approach the Uniaxial Compressive Strength (UCS, or σ_c), increasing levels of damage in the form of stress fracturing (thin bands of cracks oriented tangential to the excavation surface, causing the rock to lose cohesion in this area) can be expected on the walls of the raises [7,9,13,49]. As damage to the raise walls increases, bored raises may become unsuitable due to the heightened risk of unpredictable instability.

During the excavation of the Onaping Depth internal winze, within Glencore's Craig Mine complex in Sudbury, Ontario, Canada, two in-line 3 m diameter raises were excavated from depths 1150–1440 m and from 1455 to 1915 m. After boring was complete, these raises were slashed to a minimum of 7.8 m diameter for the internal winze excavation. A long section of the site is presented in Fig. 1.

Both raises were excavated in norite, a fine to medium-grained igneous rock that is characterized as strong and brittle. The rock mass contains widely spaced and long planar/persistent joint sets (1–2 m spacing). The joints are often filled with epidote, chlorite, or other soft mineral coatings, and have limited asperities or undulation, making them prone to wedge mobilization and stress bulking. Geotechnical logging was completed on cores recovered from holes drilled near the shaft. Both the rock mass quality (Q) and the rock mass rating (RMR) were collected from all the holes. The average RMR ranged from 75 to 85 – a classification of good to very good rock mass [6,31].

Core samples of norite were collected from the drill holes and sent to the laboratory at Northeastern University, China, for mechanical property testing to obtain the complete stress–strain curves under axial-strain-controlled loading using Stiffman [11]. Uniaxial Compressive Strength (UCS) tests were completed to determine the elastic deformation properties (Young's modulus and Poisson's ratio), and Triaxial Compressive Strength (TCS) tests were completed at confinements of 0.5, 1.0, 2.5, 5.0, 10.0, and 15.0 MPa to determine the complete stress–strain curves and residual strength of the rock. A total of 45 samples were tested. The average UCS was 225 MPa and the average Young's modulus was 54 GPa.

After completion of each of the bored raises, high-precision LiDAR scans were obtained to assess the rock mass response from the bored excavations. On average, the 3 m diameter raises grew by 0.45 m on both the North and South walls (Fig. 2a & c) if the effect of faults and the influence of the bottom of the raises are discounted. Based on empirical assessments, this amount of breakout was expected and was operationally manageable with the shaft sinking arrangement. The operational plan was to place a 3 m diameter plug on top of the raise, which would allow operators to work on the bench and protect them from the open hole hazard.

When the bored raises were complete, there was a rapid reduction in seismic activities throughout the raise with all activity stopping after two weeks, which indicates the raises had stabilized. The 1455–1915 raise remained idle for over a year before slashing reached that level, with no recorded instability on the seismic system or visual evidence of rock failure at the bottom. However, when slashing began in each raise, there was a rapid notch growth throughout the entire length of that raise.

After slashing down 100 m in each of the raises, another set of LiDAR scans was conducted. These scans revealed an average notch growth of 2–2.2 m, resulting in an overall width of 7–7.4 m notch tip to notch tip (Fig. 2b & d). This rapid notch growth was not anticipated and presented significant operational challenges. Although the initial growth was rapid, it slowed and eventually stopped or slowed to the extent that no meaningful growth was observed beyond the limits of the second scan. This conclusion was based on occasional LiDAR scans conducted throughout the shaft slashing process.

An in-depth investigation of the raises revealed four mechanisms of

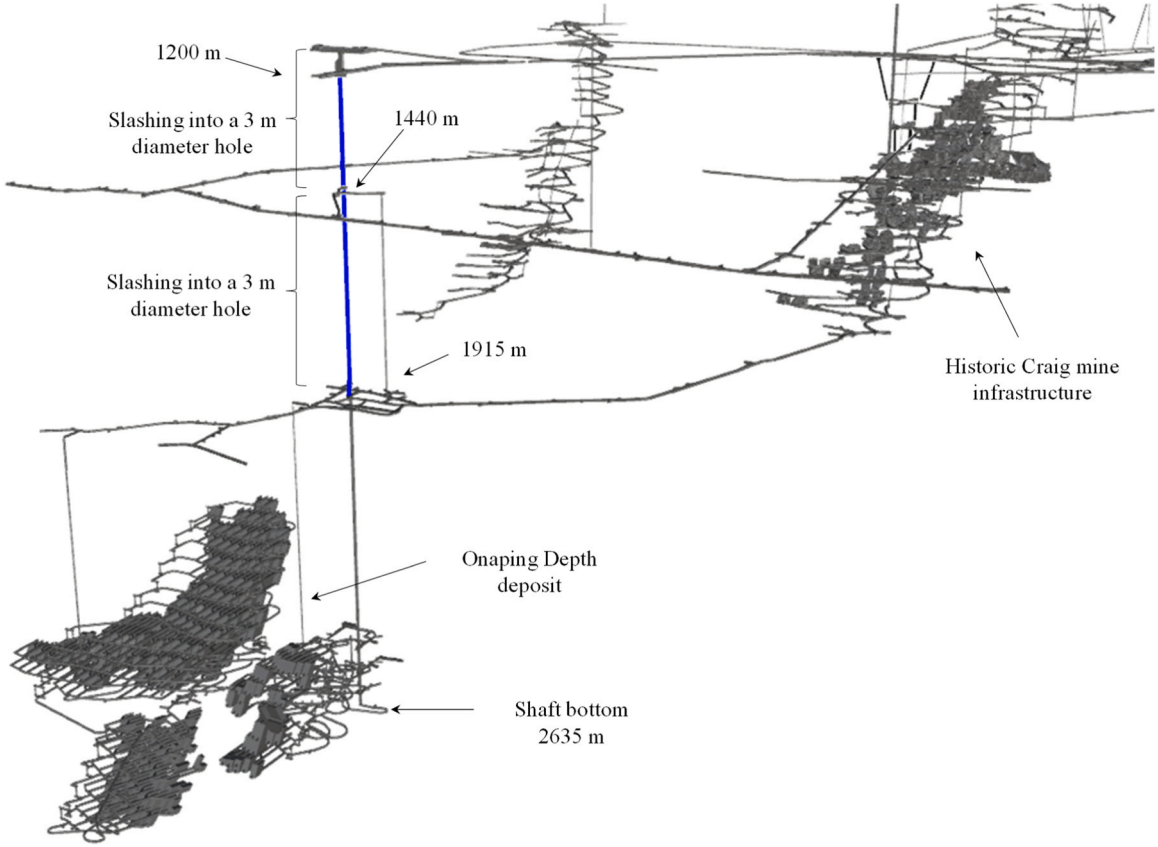

Fig. 1. Long section of Craig Mine with the Onaping Depth deposit. Blue excavations are the focus of this paper.

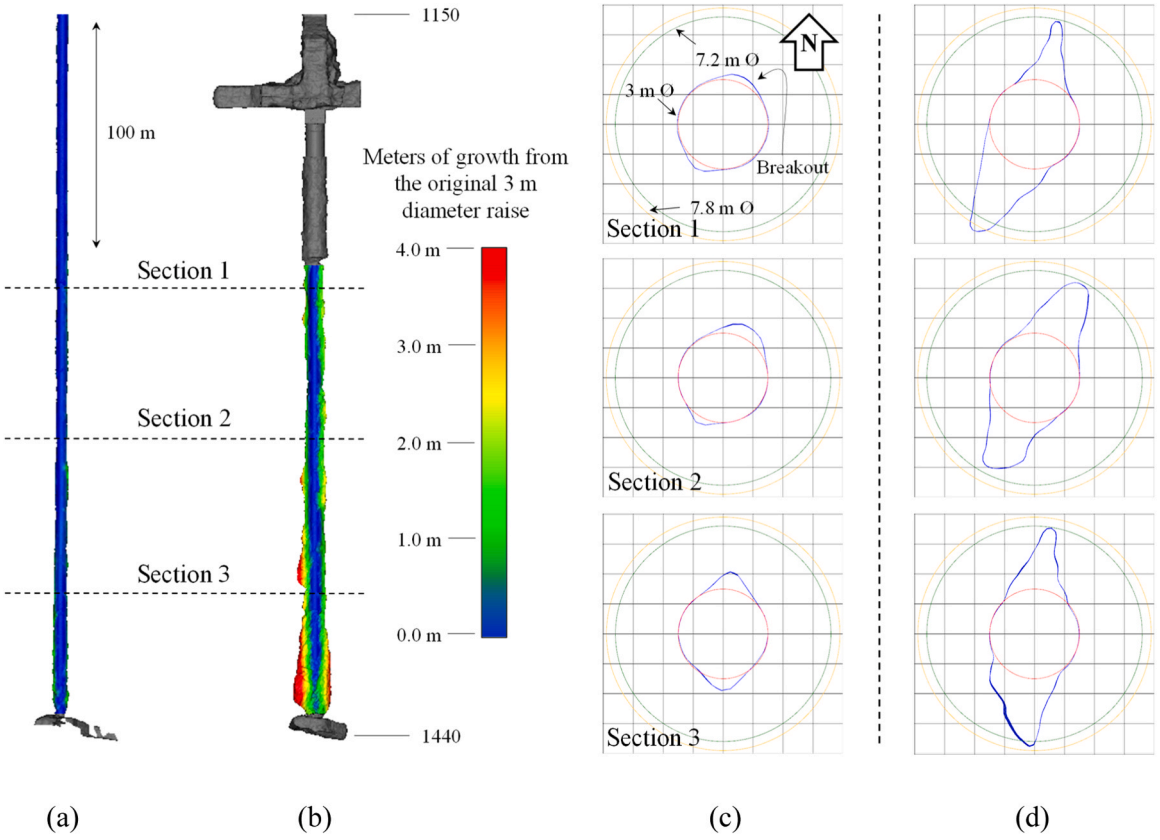

Fig. 2. (a) The LiDAR scan of the raise prior to beginning slashing, (b) the LiDAR scan of the raise after slashing down 100 m, (c) 10 cm thick plan view slices of the raise before slashing occurred, and (d) 10 cm thick plan view slices of the raise after slashing down 100 m. Note: the location of the section slices in (c) and (d) correspond with the section notes in (a) and (b).

deterioration leading to notch growth: stress-driven failure, influence of structures, scouring by falling material during mucking, and mining-induced failure from slashing stress redistribution [25,26].

The source mechanism of deterioration in the raises was stress fracturing, which occurred on the North and South walls due to the East-West orientation of the maximum principal stress. Using $\sigma_1 = 1.8\ \sigma_3$ for the field stresses, the ratios of maximum tangential stress to the average UCS strength of norite (225 MPa) are 0.62 at 1150 m, 0.77 at 1200 m, and 1.00 at 1915 m. Overstress on the North and South walls of the raise was the underlying factor that led to notch growth with other mechanisms exploiting the stress fracturing leading to further notch growth in the raises.

Scouring occurs when falling rocks impact the walls of a raise causing some damage and removal of the rock. Scouring was found to be the greatest factor leading to growth in the raises; however, the effect of scouring was exacerbated by the presence of stress fracturing. Initially, as the raisebore advanced, the relatively small, bored cuttings did not result in significant notch growth due to their small size ($<$ 10 cm or a few kg), resulting in low kinetic energy when impacting the walls. This is why the largest depth of failure was 0.45 m in this construction stage. Due to the weakened and fragile state of the stress-fractured rock, any external influence, such as impact from large falling rocks, will result in the preferential removal of the notch material. The resulting removal of confinement from the notch allows the stress fracturing process to extend deeper. As slashing occurred and larger broken rocks fell down the raise, the scouring mechanism became the dominant factor leading to notch growth.

Initially, the notch growth in the raise occurred rapidly due to the larger surface area available on the intact raise for stress fractures to develop. However, as the notch tips tapered to a narrower geometry, the stresses at the tips intensified but decreased in surface area. The intense stress fracturing became highly localized and the probability of falling rocks reaching the notch tips to scour the fractured rock decreased. In addition, as the notch narrowed, there was an increase in confinement on the notch tips, which helped stabilize the notches.

The study presented in this paper examines the empirical and numerical modeling methods to predict the depth of failure (notching) in the raises excavated at Onaping Depth. An innovative approach is presented to simulate the progressive failure that was observed in the raises with FLAC3D, considering the failure mechanisms of stress-driven failure and scouring. The following sections are arranged as follows: Section 2 examines the empirical depth of failure and compares what was observed in the Onaping Depth raises, and Section 3 presents the numerical method and simulation results. Discussions and conclusions are presented in Sections 4 and 5, respectively.

2. Estimation of depth of failure and notch growth

2.1. Empirical assessment of depth of failure

One of the well-known cases of brittle rock failure in underground excavations was the horizontal Mine-by Tunnel experiment in the Underground Research Laboratory (URL) at Pinawa, Manitoba, Canada. The 3.5 m diameter tunnel, located at a depth of 420 m below the surface, had a slow progressive failure that occurred in the roof over five months as a result of stress fracturing [55]. The slow progressive failure manifested as spalling and resulted in a 0.525 m deep notch forming on the back. This spalling failure has been studied by numerous researchers [15,17,52,54]. The excavation was completed in massive brittle granite, which was unjointed, stiff, and strong with a UCS of 213 MPa [49].

In civil engineering, brittle rock failures in large-diameter bored holes have been observed in a field experiment at the Äspö Hard Rock

Laboratory in Sweden [2]. It was found that stress-induced notching around the excavation preferentially followed the foliation of the granite host rock [14]. Violent strainburst failures have also been studied in the tunnel boring machine excavations at the Jinping II hydropower station in China, which resulted in notch formation [21]. In both cases, the types of failure could be predicted based on test results from laboratory experiments.

Based on the observations from the Mine-by experiment, several studies were completed to estimate the depth of failure around excavations in the 1990s [41,49]. The results of the Äspö pillar project as well as other bored raises have been added to the work, resulting in further refinement of the empirical relation for the prediction of depth of failure [51].

The empirical estimation is based on the Kirsch solution which calculates the maximum tangential stress on the boundary of a circular excavation ($\sigma_{max} = 3\sigma_1 - \sigma_3$). The equation depends on the principal stress components in the plane of interest. Based on the empirical relation $\frac{d_f}{a} = 1.25\frac{\sigma_{max}}{UCS} - 0.51(\pm 0.1)$, where a is the radius of the excavation and UCS is the laboratory uniaxial compressive strength, the maximum expected depth of failure (d_f) can be estimated [53]. Several other equations have been derived based on different strength factors, including those specifically formulated for determining the spalling limit [51]. These equations are based on fitting data from the case studies that have been completed. The maximum depth of failure can be estimated based on the linear best-fit line. Fig. 3 presents the measured breakout (dots) and the predicted breakout (lines) for stress-to-strength ratios ranging from 0.4 to 1.2.

At Onaping Depth, using the formula above with the vertical stress $\sigma_3 = \sigma_z = 0.027\,H$ (MPa), horizontal stresses $\sigma_1 = 1.8\,\sigma_z$, $\sigma_2 = 1.1\,\sigma_z$, where H is the overburden depth in m, and a UCS of 225 MPa for norite, the largest notch depths calculated along the raise are 0.35, 0.63, and 1.09 m at the 1150, 1440, and 1915 levels, respectively. Another generalized stress assumption that is based on data collected from numerous mine sites within the Canadian Shield is as follows: $\sigma_1 = 13.5$ MPa + 0.0344 H MPa/m, $\sigma_2 = 8.0$ MPa + 0.0233 H MPa/m, $\sigma_3 = 3.0$ MPa + 0.0180 H MPa/m [3]. Based on this assumption, the largest notch depths calculated along the raise are 0.32, 0.52, and 0.85 m at the 1150, 1440, and 1915 levels, respectively. Kaiser and Maloney [42] proposed three stress domains for the Canadian Shield based on depth below surface [42]: Domain 1 for shallow depth where stresses are influenced by historic unloading processes, Domain 3 where the stresses are undisturbed at greater depths, and Domain 2 as the boundary between the other two. The field stress for Domain 3 (below 600–1500 m) is $\sigma_1 = 23.636$ MPa + 0.026 H MPa/m, $\sigma_2 = 17.104$ MPa + 0.016 H MPa/m, and $\sigma_3 = 1.066$ MPa + 0.020 H MPa/m. Based on this field stress assumption, the largest notch depths calculated along the raise are 0.33, 0.48, and 0.74 m at the 1150, 1440, and 1915 levels, respectively.

Aside from the bottom of the raise, notching in the 1150–1440 segment of the raise was in line with the estimate based on the field stress assumptions stated above, where the influence of the 1440 level caused increased notch growth. Overall, the measured breakouts better matched the estimate using the Kaiser and Maloney [42] stress assumption for Domain 3 with a lower stress magnitude. However, both the base case and Arjang and Herget [3]'s empirical assessments overestimated the depth of failure in the 1440–1915 raise. Kaiser and Maloney [42]'s Domain 3 magnitude provides a better overall fit for the entire length of both raises, but the stresses are overestimated with increasing depth. As a result, the locked-in σ_1 stress component of 23.636 MPa was reduced to 19.636 MPa, which is within the + /- 11.556 MPa range. Table 1 presents a summary of measured breakout depths and the empirical estimates of breakout depths for the entire length of the Onaping Depth raises. Breakouts in the raises were classified based on field observations and inferred mechanisms.

Fig. 4a presents the measured breakout depths at 10 m intervals along the entire length of both raises from 1150 to 1915 m before slashing occurred. In the top 120 m of each raise, limited notch growth was observed. It is inferred that raisebore cuttings in freefall do not have sufficient kinetic energy to induce meaningful notch scouring until they approach a terminal velocity. After 120 m of freefall, the cuttings are approaching the terminal velocity (50–70 m/s depending on assumptions) and have sufficient kinetic energy to knock material loose. As rocks travel further down the raise, the probability of a rock hitting the fractured rocks increases as the cumulative amount of cuttings increases. Finally, there was an increased depth of failure noted at the bottom of both raises where there was the influence of the excavations below. Faults were encountered in both of the raises, and they also influenced the depth of failure (Fig. 4). The fault encountered in the 1440–1915 raise was sub-vertical, resulting in exposure over a longer distance. On the other hand, the fault encountered in the 1150–1440 raise was sub-horizontal, which was only encountered in a few rounds.

Fig. 4b compares the notch growths in the raises when boring was completed with those after slashing down approximately 100 m. There was less growth after slashing down 100 m in the 1440–1915 raise for several reasons: 1) the 1150–1440 raise had a significant amount of larger rocks pass through as a result of excavating the large headframe excavation; 2) there was a highly competent section of ground in the 1440–1915 raise where the rock strength was higher, leading to less growth; and 3) an 8 m diameter inverse raise was blasted at the bottom of the 1440–1915 raise, which reduced the restriction point, thereby preventing a large void from forming (like what occurred at 1440). Due to these reasons, the notch failure in the 1150–1440 raise will be the focus of this paper.

The calculated depths of failure are also plotted in Fig. 4 as a blue line for the stress assumption of $\sigma_1 = 1.8\,\sigma_z$ and $\sigma_2 = 1.1\,\sigma_z$, a green line for a generalized stress assumption based on the data collected from some mine sites within the Canadian Shield [3], and an orange line for Kaiser and Maloney [42]'s Domain 3 stress assumption [42]. The Kaiser and Maloney [42] stress assumption was used for the remainder of this research.

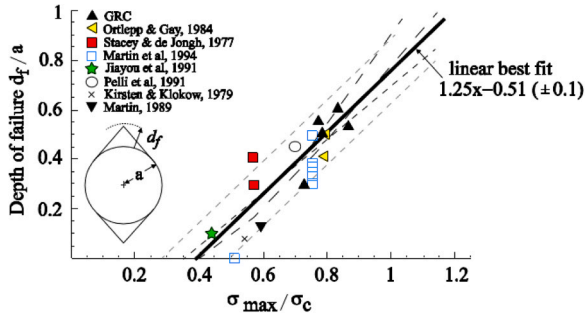

Fig. 3. Empirical relation for determining depth of failure around a circular excavation [41,49].

2.2. Numerical modeling of depth of failure

Numerical models are used by geomechanical engineers to predict rock mass responses to mining activities. The models can vary in complexity depending on the fidelity of the inputs and desired solution accuracy. Compared with the trial-and-error approaches, the use of numerical modeling is beneficial because several different scenarios and input conditions can be tested and compared with field observations to allow for an understanding of the sensitivity to critical factors and establish behavior trends. In general, there are three categories of numerical methods used in rock mechanics and rock engineering: continuum, discontinuum, and hybrid methods [39].

The continuum and discontinuum methods have their own advantages and disadvantages. Continuum models use deformable bodies to represent the behavior of rock masses and assume that a rock mass is a

Table 1
Summary of measured and empirical estimates of breakout depths.

Depth (m)	Field observation	Measured depth of failure (m)	Calculated fepth of failure (m): $\sigma_1 = 1.8\sigma_z$, $\sigma_2 = 1.1\sigma_z$	Calculated depth of failure (m): Canadian Shield [3]	Calculated depth of failure (m): [42]
1160–1270	Limited scouring	0.31	0.36–0.46	0.33–0.40	0.23–0.29
1280–1370	Increased scouring	0.43	0.47–0.56	0.41–0.47	0.29–0.34
1380–1440	Bottom of the raise	0.81	0.57–0.62	0.48–0.52	0.35–0.38
1460–1580	Limited scouring	0.26	0.65–0.76	0.54–0.62	0.39–0.45
1590–1620	Increased scouring	0.50	0.77–0.80	0.63–0.65	0.46–0.48
1630–1720	Influence of a fault	0.88	0.81–0.90	0.65–0.72	0.48–0.53
1730–1830	Increased scouring	0.49	0.91–1.01	0.72–0.79	0.53–0.59
1840–1910	Bottom of the raise	1.28	1.02–1.08	0.80–0.85	0.59–0.63

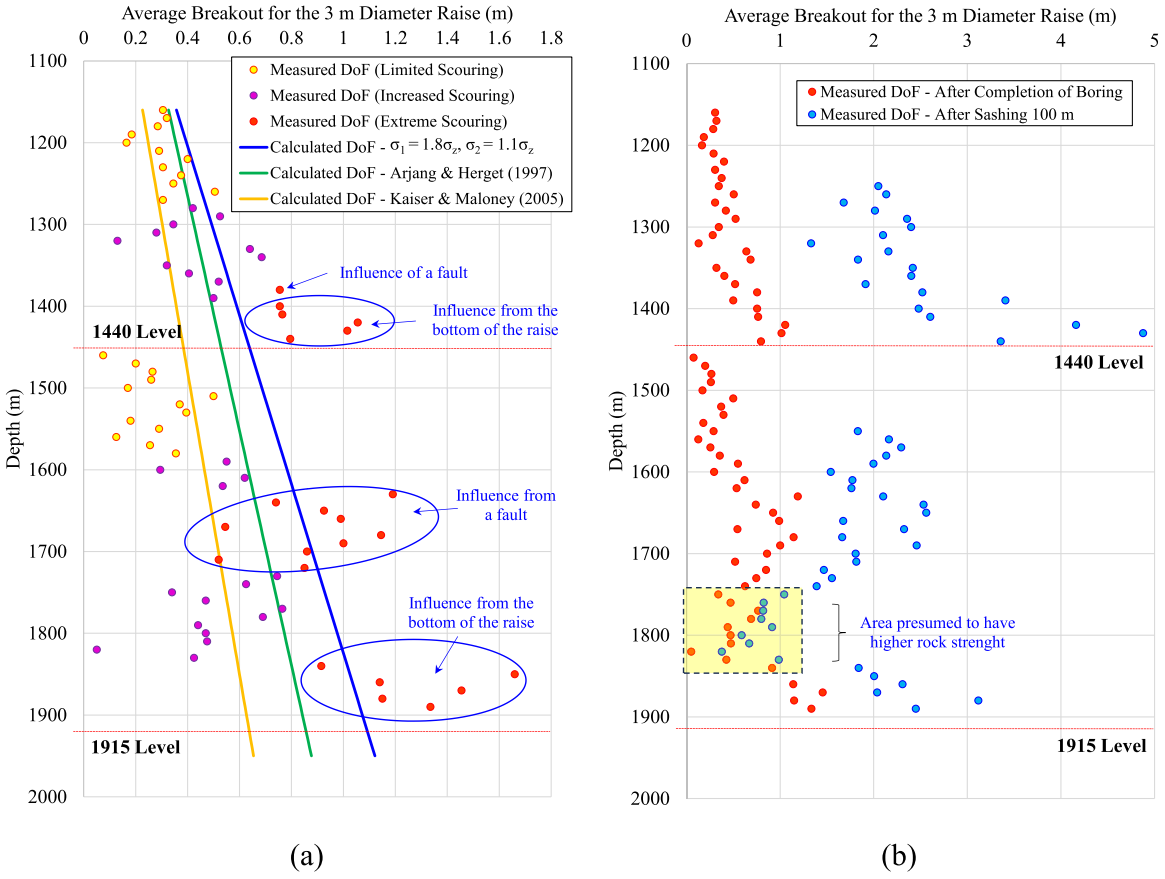

Fig. 4. (a) Average breakout depths measured at 10 m intervals from the LiDAR scans of both raises with the empirical estimates plotted at corresponding depths. (b) A comparison of breakout in the raises after boring was completed and after slashing down 100 m in each raise.

solid, continuous body without explicitly accounting for fractures or structural discontinuities. In contrast, discontinuum models specifically account for discrete fractures and the interaction between individual blocks of the rock mass [8]. Continuum models represent non-linear material response using non-linear constitutive laws, while discontinuum models explicitly model the deformability of discontinuities. The inclusion of discontinuities introduces complex non-linear response due to slip and separation of individual blocks in the model.

Continuum methods can not explicitly simulate fracture growth or allow failed elements to detach. Instead, they rely on constitutive models to determine the stresses and strains within an element. Although discontinuum methods may appear to be superior by allowing the simulation of large deformation and detachment between blocks, which could replicate stress fracturing and slabbing around excavations, the intensity of stress fracturing is influenced by the element size and is usually underrepresented. In addition, as displacements and velocities increase in a discontinuum model, the time step decreases significantly, increasing model run time. Hybrid numerical methods combine continuum and discontinuum components, allowing for a smooth transition from continuum to discontinuum, taking advantages of both methods at different scales. However, the explicit modeling of rock fracturing remains challenging due to the reasons stated above.

Constitutive models can be user-defined but are generally built into the codes. Constitutive models are selected based on the behavior of the

material being simulated. It is important to select an appropriate constitutive model to simulate the conditions being investigated. Elastic models cannot accurately simulate conditions near the excavation boundary as they do not capture plastic deformations of rock. This limitation makes them unsuitable for simulating depth of failure, where plastic deformation plays a critical role [60]. Elasto-perfectly-plastic models can capture plastic deformation with increasing strain; however, they are not suitable for brittle rock failure simulation as they underestimate the depth of failure due to high residual strength [15,23,55].

Several studies used FLAC3D to examine rock mass response of tunnels excavated using tunnel boring machines (TBM). Nozari and Khosravi [57] used FLAC3D to predict the stability of the Alborz tunnel passing through the Kandovan fault zone. Abdollahi et al. [1] used FLAC3D to simulate the response of a TBM-excavated Safaroud water transmission tunnel so that suitable reinforcement strategies could be selected. Hasanpour et al. [27] examined the TBM entrapment while advancing due to adverse geological conditions with FLAC3D. Zhou et al. [71] established a hydro-mechanical coupled model in FLAC3D to investigate the interactions between the TBM machines and surrounding rock under high stress and water pressure during the excavation of a deep tunnel.

The Mine-by tunnel has received noteworthy attention due to the large amount of high-quality data collected in the project. In general, numerical models on the Mine-by tunnel were calibrated based on the observations of the depth of failure. Martin [48] theorized that brittle rock failure is a process where cohesion is gradually lost with the onset of tensile fracturing as the rock is loaded, while friction is mobilized in the fracturing process [48]. A cohesion-weakening and frictional-strengthening (CWFS) model was developed and implemented in FLAC, where the model parameters were assigned as a function of plastic shear strain [24]. The CWFS model was able to simulate the overall notch geometry observed at the Mine-by tunnel experiment. Based on the cohesion and friction strengths used in the models, the scaled rock mass UCS was 100 MPa.

Diederichs et al., [16] used a set of spalling parameters and calibrated the approach based on the notch failure observed in the Mine-by tunnel experiment. Using the Hoek–Brown failure criterion with two envelopes representing the peak and residual strengths in PHASE2 (RS2), the notch profile of the Mine-by tunnel was captured. As per the spalling criterion, elements that reach peak strength in areas of low confinement, such as around an excavation, exhibit a perfectly brittle behavior, meaning that the strength drops from the peak to the residual strengths instantly. In areas of high confinement, the rock shows a perfectly strain-hardening behavior, meaning that the strength increases instantly from the peak to the residual strengths because the "residual strength" defined by the given spalling parameters is higher than the peak strength when the confinement is high. The peak strength, defined by UCS = 235 MPa, and the Hoek–Brown failure criterion parameters of $m = 1$, $a = 0.25$, $s = 0.033$, results in a peak strength envelope similar to that of the CWFS model with a rock mass UCS of 100 MPa. At a confinement of 30 MPa, the peak strength is about 175 MPa but the "residual strength" is about 220 MPa.

Vazaios et al. [64] used Irazu software, a hybrid finite-discrete element method code to simulate brittle rock fracturing observed in the Mine-by tunnel experiment [64]. Three scenarios were run with varying in-situ stresses and a rock mass UCS of 120 MPa. The modeling results demonstrated that failure occurred when the maximum principal stress at the tunnel boundary was between 40 % and 60 % of the UCS of the rock mass. Furthermore, cracks formed when confinement levels were between 1 % and 4 % of the UCS of the rock mass. The depth of failure simulated in the model closely matched the failure profile observed in the field. Examples from the CWFS model and the Irazu model for simulating the depth of failure observed in the Mine-by tunnel experiment are presented in Fig. 5b and c.

Hoek, [30] conducted a numerical study of the notch development of the Mine-by tunnel using RS2 elastic analysis in combination with a composite spalling strength envelope. The analysis starts with a circular tunnel and define the zone in which fracture initiation can initiate, defined by the $\sigma_1/\sigma_3 = 20$ contours. Then, the Strength Factor contours are calculated using the Hoek–Brown failure criterion with $\sigma_c = 106$ MPa and $m_i = 15$. For the zone defined by Strength Factor < 0.93, it is assumed that the spalls are fully developed and free to fall from the roof of the excavation. A new tunnel geometry is thus determined based on the removal of the spalled zone in the roof. Based on the new tunnel geometry, a new RS2 model is built and the stress analysis is conducted and the notch growth criterion is checked. If a zone satisfies the zone removal criterion, it will be flagged and a new RS2 model based on the new notch geometry is built. The process is repeated to mimic the gradual notch growth. After 24 iterations, Hoek [30] shows that the final notch geometry resembles the field observation well. A major limitation of the approach is that it is extremely time-consuming because 24 RS2 models needs to be built. Nevertheless, it provides a new and interesting approach for notch growth simulation.

These numerical models capture the depth of failure observed in the Mine-by tunnel experiment; however, there are some issues linked to those models. The first issue is representing notch failure using yielded elements in the continuum models (see Fig. 5b). Depending on the

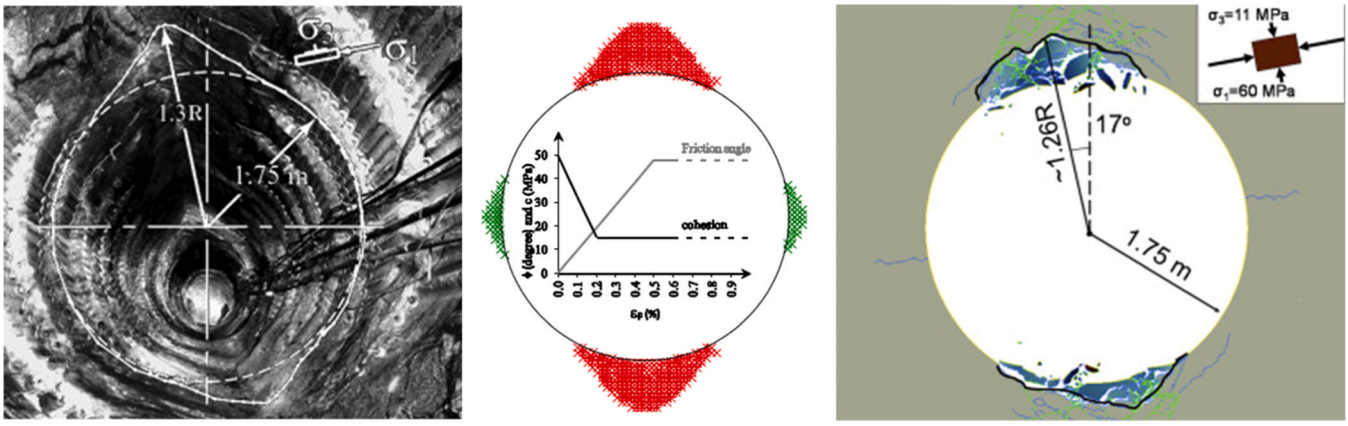

Fig. 5. (a) Image of the Mine-by tunnel experiment with notches formed [48], (b) notch formation simulated using the CWFS model implemented in FLAC [24], and (c) crack formation and mobilization simulated using Irazu [64].

residual strength model used, the stresses in the yielding zone can still be very high, which is not in agreement with the field case where the notch zones contain no fractured or yielded rocks. In other words, the simulation results are influenced not only by the peak strength, but also by the residual strength. The peak UCS used by the CWFS and the spalling models is about 100 MPa, significantly lower than the strength of the rock tested in the laboratory. The second issue is that the residual strength is higher than the peak strength in the CWFS and the spalling models when confinement is high, which contradicts the rock test data that consistently show that the post-peak strength and residual strength of brittle hard rock are all lower than the peak strength at confinements expected near excavation boundaries. The third issue is that the Mine-by tunnel was excavated using the mechanical breakage method, resulting in a non-smooth tunnel boundary (Fig. 5a). It was demonstrated by Cai and Kaiser [12] that when the non-smooth Mine-by tunnel boundary is considered in the numerical model, the equivalent UCS of the rock can be as high as 175 MPa, approaching to the field strength of massive rocks without joints [12]. The underestimation of field strength can also be seen in the Irazu model [64] because UCS = 120 MPa had to be used to account for the reduced maximum principal stress acting on the smooth tunnel boundary to initiate failure.

Although those models were able to capture the notch profile observed, there are fundamental differences between the observations made in the Mine-by tunnel experiment and the deterioration of the bored raises observed at Onaping Depth. First, the Mine-by tunnel was a lateral excavation, and the notch formed in the back of the excavation was aided by gravity failure, while the notch in the floor was suppressed by the dead weight of the broken rocks in the notch. Second, the deterioration observed in the notches at Onaping Depth was progressive. Unlike the Mine-by tunnel models presented above, actual deep-seated wedges were not observed to fail and mobilize from the walls of the raises at Onaping Depth. Instead, the failure observed in the raises was progressive with thin (5–25 mm thick) stress-fractured slabs of rock oriented tangential to the excavation, falling from the walls. Third, the bored raises have smooth walls and using a smooth wall numerical model will not adversely impact the model parameter calibration. Finally, scouring-induced notch growth occurred in the vertical raise at Onaping Depth, which is not an issue in lateral excavations, such as the Mine-by tunnel.

During the shaft slashing process, blast holes were drilled around the 3 m diameter raise in each 5 m long development round. Then, the holes were blasted and the rock was slashed into the 3 m diameter raise and collected at the bottom. With each blast, the newly exposed floor (bench) revealed a cross-section of stress-induced damage that had developed in the walls of the raise prior to being exposed. In general, stress fracturing was limited to 10–20 cm deep into the walls, in the direction perpendicular to the maximum principal stress orientation. Stress-fractured slabs, about 0.5–25 mm thick, comprise the overall 10–20 cm thick package. These slabs were dislodged piece by piece as falling rocks impacted them. As the stress-fractured rocks were removed from the walls, the reduction in confinement enabled deeper material to reach its peak strength, leading to the formation of new fractures. This process perpetuated the 10–20 cm stress-fractured rock thickness. This 10–20 cm thickness of stress fracturing was observed in the top 50 m of both raises, where the influence of scouring would be limited. Throughout the rest of the raise where the influence of impact of falling rocks became more dominant, the stability of the fracture zone was continuously changing, masking the purely stress-driven processes.

As far as the authors know, there have been no established methods in numerical modeling to account for the effect of stress fracturing and subsequent scouring in vertical shafts. This challenge is addressed in this study. We proposed a new methodology to handle both stress-induced and impact-induced notch growth in vertical shaft construction in the next section.

3. Numerical modeling of notch failure in a bored raise

3.1. Selection of numerical modeling code

The modeling goal is to replicate the failure behavior that was observed in the raises. Thin zones of stress-damaged rocks formed on the critically stressed walls would remain in place if undisturbed, allowing the excavation to stabilize. However, when these stress-damaged zones were removed by external influence such as scouring, additional stress-damaged rock would form, initiating a repeating cycle of disturbance, fracture growth, and re-establishment of equilibrium state. An example of the complexity of the deterioration mechanisms observed in the Onaping Depth raises is presented in Fig. 6. Falling rocks impact the raise walls during the slashing process, which is represented by the recorded microseismic events.

Two methods were considered for simulating notch growth in the Onaping Depth raises – continuum and discontinuum methods. A discontinuum method code can simulate displacements of individual blocks; however, the problem to be simulated is highly complex. If scouring is considered, the mass, velocity, and trajectory of falling rocks impacting the walls must also be simulated along with the stress fracturing damage. Replicating these deformation processes in discontinuum codes presents significant challenges and complexities. In addition, as more fractures are considered along with falling blocks, the simulation time and computational requirements become unmanageable.

The combination of the two different but linked failure mechanisms (stress fracturing and scouring) poses significant challenges for continuum-based codes. This difficulty arises from the inability of the continuum method to simulate fracture formation and the subsequent mobilization of blocks. If a continuum code is used, the conditions necessary for fracturing and scouring to occur must be represented in the elements. Given the overall goal of simulating the emergent behavior of the notch growth in the raise, the complexities associated with explicitly simulating actual fractures, mobilized rocks, and scouring were deemed unnecessary. Therefore, the continuum method was selected for this study.

Itasca's FLAC3D code was selected to simulate the deterioration in the bored raises at Onaping Depth. FLAC3D is a three-dimensional explicit Lagrangian Finite Difference Method code. Materials are represented by elements or zones within a three-dimensional user-defined and populated grid. Elements within the model respond to applied forces and boundary conditions according to a prescribed nonlinear stress–-strain relation. This code allows accurate simulation of post-peak strength loss using advanced strain-softening models [37].

There are many pre-defined constitutive models in FLAC3D. However, for simulating notch growth in brittle rock, a constitutive model that allows for direct user control of the peak and post-peak properties is needed. For this reason, the Strain Softening Ubiquitous Joint (SUBI) model was selected. This model provides the flexibility to independently control post-peak parameters based on the accumulated plastic strain.

To demonstrate the capacity of the SUBI model, simulations were first conducted to simulate the unconfined and confined pre-peak and post-peak behaviors of the rock, using test results obtained from the laboratory tests conducted by Northeastern University in China.

3.2. Defining peak and post-peak strength parameters based on laboratory test results

The complete stress–strain curves of the laboratory samples were replicated numerically using a one-zone model. Compared with explicitly replicating the cylindrical shape of samples used in a physical laboratory test, using a one-zone model has advantages such as rapid convergence, simplified boundary conditions, and uniform zone size and shape.

Fig. 6. (a) Images of stress fracturing around the tip of the notch and (b) a 24-hour mining cycle with recorded microseismic events showing rock falling and impacting the walls of the raise.

The calibration process started with an initial set of material properties that were based on the properties derived from the laboratory tests, then fine tuning the input parameters (elastic modulus, cohesion, and friction) and the critical strain to match the modeling results with the laboratory data. After extensive trial-and-error model simulations, a set of calibrated parameters was derived and presented in Table 2, along with the initial properties derived from the laboratory test data. The peak strength is controlled by the cohesion and frictional strength. The modulus of the rock is defined by the slope of the stress–strain curve in the elastic deformation region. The slope of the stress–strain curve from the peak to the residual strengths is controlled by the critical strain. The ultimate residual strength properties are defined by the residual cohesion and frictional strength. In SUBI models, joints can either be turned off or they can be assigned with high strength properties to ensure they remain elastic. For this study, the joints were turned off.

The UCS of norite obtained from the laboratory test is 225 MPa, while the calibrated material properties used in the FLAC3D simulations have a UCS of 208 MPa (derived from $UCS = 2c\cos\phi / (1 - \sin\phi)$, where c is cohesion and ϕ is the friction angle of the rock). Fig. 7 presents the strain-softening model for the numerical simulation. A comparison of the laboratory test and the FLAC3D numerical modeling results is presented in Fig. 8. Overall, there is a good agreement between the laboratory results and the modeling results across a range of confinements in both pre-peak and post-peak deformation stages. It demonstrated that the selected model properties accurately represented the rock's strength behavior across a range of confinements. Therefore, it was deemed acceptable to proceed to the raise-scale model based on these material properties.

Table 2
Material properties derived from the laboratory experiments and the material properties used to simulate the testing in FLAC3D.

	Laboratory experiments			FLAC3D simulation		
	Peak	Residual	Critical strain	Peak	Residual	Critical strain
Young's modulus (GPa)	53.95	53.95	-	45.86	45.86	-
Friction angle (°)	55.4	42.6	0.13–0.18 %	48.4	42	0.11 %
Cohesion (MPa)	37.4	0.2	0.13–0.18 %	39.5	3.8	0.09 %

3.3. Scaling laboratory rock properties to a 3 m diameter raise and calibration of material properties based on stress-induced damage in the raise

The results of laboratory testing are not suitable for representation of the rock masses at larger scales [29]. As larger volumes of rock mass are considered, the potential defects, such as joint sets, faults, micro-cracks, grain size, etc. must also be considered. Due to the existence of defects within a large volume, rock mass strength and stiffnesses are lower at larger scales, which need to be properly scaled based on the laboratory test results and field monitoring data.

Scale dependency of rock mass strength and stiffness is an important issue in geotechnical engineering [29,33,61,67]. The representative volume element (RVE) has been suggested by many researchers as a means of scaling the material properties to the excavation size [35,46,56,58,59,62,65,66,68]. Based on the scale of the simulation model, a 3 m diameter raise that grows to 7 m, the rock mass strength is estimated to be 0.4–0.5 of the intact rock strength. Therefore, with an intact strength of 208 MPa for norite (derived from the laboratory scale calibration modeling), the rock mass strength for the raise is estimated to be 83.2–104 MPa for the scale of the raise. Based on a series of test model runs, the rock strength used in the raise model was downgraded to 104.5 MPa with the SUBI material properties presented in Table 3. The critical strains are slightly larger than those for the intact rock. As can be seen in the results presented in the next sub-section, these model parameters capture the stress-induced notch failure well.

3.4. Simulation of notch failure in bored raise without scouring damage

The grid to represent the raise is 60 m long by 60 m wide and 10 cm thick with an inner region of 14 m × 16 m centered around the raise with high density zoning. The mesh is effectively a 2.5-dimensional model where some out-of-plane influence is accommodated without the full representation of the vertical extents of the raise. The model was constructed using deformed hexahedral mesh in Griddle, an advanced meshing tool created by Itasca [38]. Plasticity resulting from tetrahedral zones is not as accurate as hexahedral or higher order zones [5,22,47]. The mixed-discretized hexahedral zones provide a better accuracy for problems involving failure and collapse of the intact block (which is the case for the notch growth simulations) and are more accurate when simulating plastic deformation of the intact material [37]. The maximum zone edge length was 8 cm with a higher density in proximity

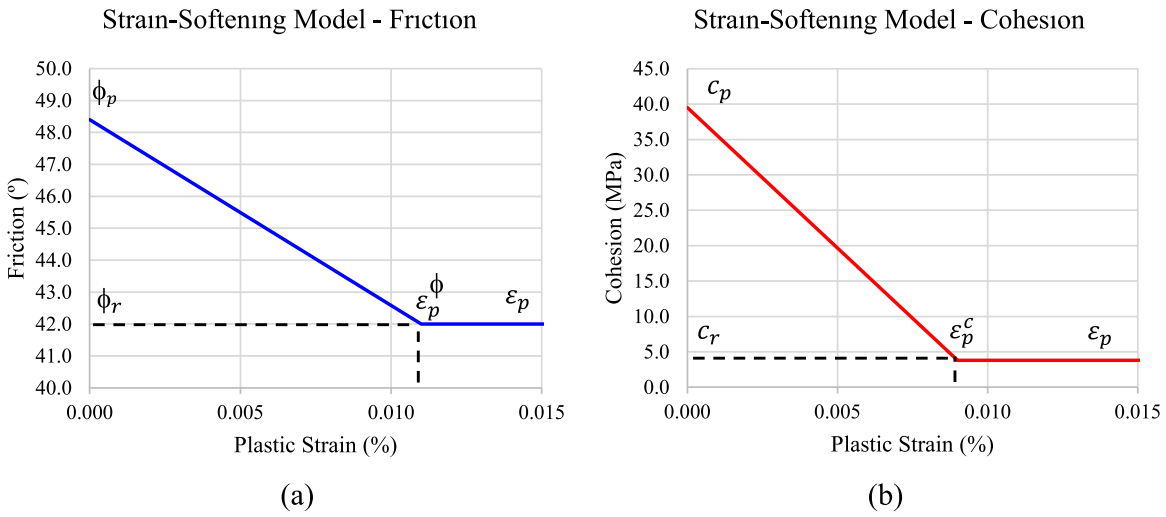

Fig. 7. The strain-softening model for the laboratory test result simulation: (a) friction angle and (b) cohesion.

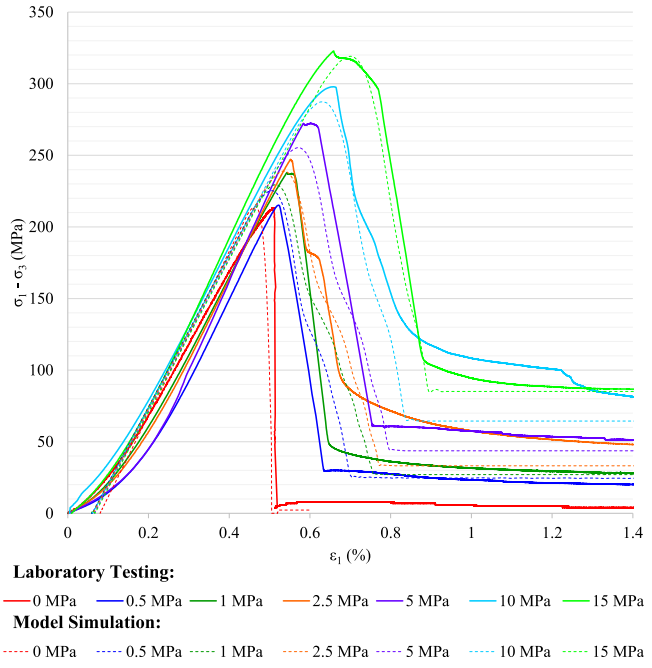

Fig. 8. Comparison of the laboratory testing and the FLAC3D model simulation results.

Table 3
Material properties for the raise simulation.

	Peak	Residual	Critical strain
Young's modulus (GPa)	44.95	44.95	-
Friction angle (°)	51	5	0.13 %
Cohesion (MPa)	18.5	0.5	0.11 %

to the raise and grading outwards to the model boundaries. In the middle of the model, a 3 m diameter cylinder was generated to represent the raise (Fig. 9). The final mesh consisted of 660,320 zones. The far field boundaries were fixed and the top and bottom surfaces were fixed in the vertical direction but allowed to move in-plane.

Notching in the raises occurred on the North and South walls, which is consistent with an East-West maximum principal stress orientation. Again, based on the measured breakouts recorded throughout the raises prior to slashing, the Kaiser and Maloney [42] stress magnitude assumption [42], which appeared to fit the observation results the best, was used for this study. As noted previously, the 1150–1440 section of the raise is examined in this study with the calibration points based on the scans presented in Fig. 2. In particular, the model is calibrated to the 1240, 1340, and 1440 elevations. Based on the calibration at these levels, the model is used to simulate the notch growth at the 1915 elevation, where the stresses are higher. The field stress assumption and the principal stresses at these elevations are presented in Table 4. σ_1 is oriented in the East-West direction and σ_3 is in the vertical direction.

The "zone relax" command in FLAC3D was used to excavate the initial raise shape. This method was chosen because it progressively reduces the stress, stiffness, and densities of the excavated material, allowing for a controlled removal of energy from the system and preventing numerically driven plasticity [10]. The process better aligns with the slow progressive excavation process of bored raises (cutting the rock) [37], [4,19,20,43,63]. If an excavation is excavated instantaneously (more akin to a drill-and-blast method) there is some numerically simulated damage in the walls of the raise which was not observed in the field. As shown in Fig. 10a, the passive excavation method is reinforced with the cutting marks visible on the East and West walls of the raise with no visible stress fracturing in these areas. The blasting-induced damage [32] was discounted for the bored raise analysis because of the nature of the bored excavation.

In FLAC3D, the yield state or zone state marker can be used to identify zones whose stresses have reached the peak strength. This is one of the most widely used indicators of instability in numerical modeling, forming the basis for various studies on depth of failure [28]. However, yielding of rock will not necessarily lead to complete failure, especially if the confinement is high [40]. In the extreme case when a perfectly plastic model is used, a yielded element can sustain the peak stress as it deforms. A yield flag alone indicates that the peak strength of the rock was reached; it provides no information about the degree of strength loss that may have occurred in the post-peak deformation stage.

For this study, a cohesion loss threshold was used to identify elements that experienced some degrees of stress fracturing initially. The cohesion did not need to be degraded completely to the residual value but a reduction from peak level was necessary. The loss of cohesion is directly related to the increase in plastic strain, but cohesion provides a more intuitive visual indicator of strength loss compared with plastic strain.

The criterion uses an iterative element removal process based on cohesion loss. Elements that meet the cohesion threshold are removed and the model is cycled until a stable state is reached. Once the stable

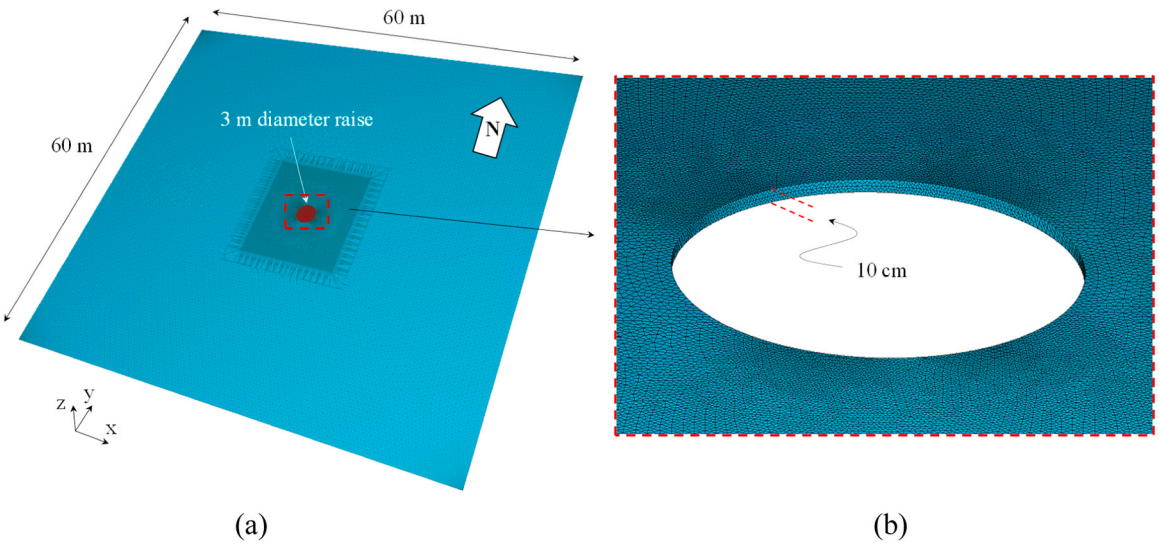

Fig. 9. (a) Isometric of the model and (b) with the 3 m diameter raise removed to show the thickness of the model.

Table 4
Summary of field stresses used in this study.

	σ_1 (MPa)	σ_2 (MPa)	σ_3 (MPa)
Kaiser and Maloney [42] Domain 3	23.636 [± 11.556] + 0.026 [± 0.012] *H*	17.104 [± 10.538] + 0.016 [± 0.010] *H*	1.066 [± 8.247] + 0.020 [± 0.008] *H*
Modified field stress for this study	19.636 + 0.026 *H*	17.104 + 0.016 *H*	1.066 + 0.020 *H*
Field stress at 1240 m	51.876	36.944	25.866
Field stress at 1340 m	54.476	38.544	27.866
Field stress at 1440 m	57.076	40.144	29.866
Field stress at 1915 m	69.426	47.744	39.366

state is reached, the element isolation routine is repeated, and the next set of elements are removed if the conditions for removal are met. Initially, the cohesion threshold for element removal is high, but as the depth increases, the threshold is lowered to account for the more random interlocking of stress fractures until no elements are removed and the system is deemed stable. Based on trial-and-error simulations to replicate the raise simulations presented in Fig. 2, a criterion was developed and is presented in Fig. 10c. The contour of cohesion after the bored raise has been completed and the profile of the raise after the initial growth criterion has been applied at the 1340 elevation are presented in Fig. 10d.

As initial stress fractures develop on the North and South walls, the stress-fractured zone is highly susceptible to removal due to the relationship between the stress fractures and the smooth wall of the bored raise. The presence of the smooth wall of the raise provides a single termination point for the stress fractured rocks on the excavation instead of having random interlocking and end points. This results in a greater chance of instability because the smooth wall acts as a plane of weakness along which the bulked material can slide. At the early stage of notch growth, the stress-fractured rocks would slough, spall or be knocked down from impact of the bored cuttings. However, as the notch depth reaches 20–40 cm, the random interlocking of the stress fractures increases and the influence of the raise wall becomes less, leading to notch growth. The removal of stress-fractured rocks as the notch becomes deeper requires a higher degree of failure in the rock or the influence of scouring with higher kinetic energy. Fig. 10a presents the highly susceptible stress fracturing developed after boring and Fig. 10b presents a later stage image of stress fracture growth that would require more degradation of the rock or the influence of scouring to remove the stress-fractured rocks.

The failure condition of the bored raise at the 1340 m level (the midpoint of the three elevations examined in the 1150–1440 raise) results in a slight cohesion loss from the peak levels on the critically stressed North and South walls. The rock experiencing some cohesion loss will stabilize in an equilibrium state, remain in place, and provide confinement to the rock behind it, helping to suppress further fracture growth. However, due to the fragility of the stress-fractured rocks after the bore passes, the damaged rock is likely to be removed. Therefore, a criterion was created to replicate the notch growth in the raises at this early stage before slashing started.

The simulation results show a thin skin of elements (maximum thickness 12.5 cm) with cohesion loss on the North and South walls of the raise initially. After the element removal criterion was applied, there was approximately 0.3 m of notch growth in the model (Fig. 10d). In general, this agreed with what was observed in the field, prior to drill-and-blast slashing to sink the shaft. However, this small amount of deterioration was not in agreement with what was observed after the drill-and-blast slashing began, where scouring from large blasted rocks impacted the walls and rapid notch growth occurred. To simulate notch growth when slashing occurred, a new set of criteria is proposed and presented in the next sub-section.

3.5. Simulation of notch failure in bored raise with scouring damage

3.5.1. Criteria for removing zones to simulate the effect of scouring

The model simulation presented in Section 3.4 replicates the early behavior that was observed in the raise. The single termination point of the assembly of stress fractures on the smooth wall of the bored raise results in high susceptibility of this damaged rock to bulking and removal from the impact of the bored cuttings. When the fractured material is removed (by bulking, scouring or other means), confinement is lost and the equilibrium state is disturbed, resulting in an incremental growth in damage. However, as the notches grow a short depth into the walls and the stress fractures have more random interlocking and higher stability, the susceptibility of notch growth decreases as a result of bulking or scouring from small, bored cuttings.

As slashing occurred and larger broken rocks were dumped down the raise, further damage could occur in the raise. Fig. 11 presents the notch

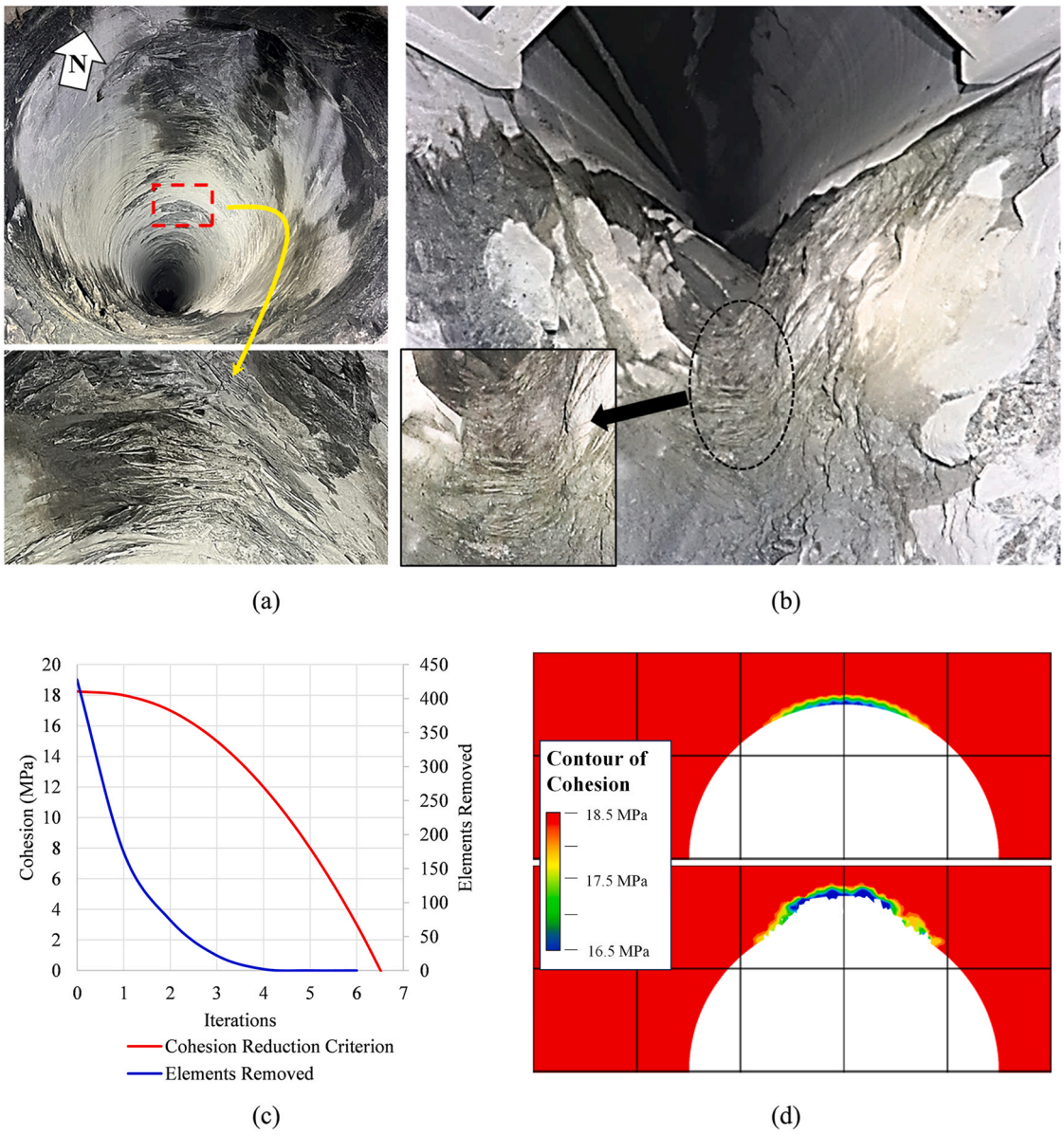

Fig. 10. (a) Initial stress fracturing visible in the raise and (b) stress fracturing as the notch grows, (c) the element removal criterion and number of elements removed at the 1340 elevation simulation, and (d) model simulation of the intact raise (top) and simulation after the element removal criterion has been applied. The 1 m × 1 m square grid (black lines) is shown for scale.

shapes at different depths as slashing and subsequent scouring occurred. At shallow depths (near the top of each of the raises) where there was no or little scouring, the depth of failure was relatively small. On the other hand, below ~100 m from the top of each of the raises where scouring could take full effect, the initial 3 m diameter raise grew to 7–7.4 m (tip to tip). The numerical model should imitate this amount of notch growth and resemble the profiles observed throughout the shaft construction.

To simulate the scouring effect from slashing (after the raise excavation was completed and the initial growth had occurred as described in Section 3.4), elements that met a volumetric strain criterion were removed in an iterative process shown in the flow chart in Fig. 12a. Once some elements were removed, the model was cycled until a new equilibrium was restored. During the process of achieving a new equilibrium, more elements could become damaged and met the criteria for removal. In that case, these elements were subsequently removed, and the process was repeated, resulting in a deep notch geometry. Larger falling rocks have a higher potential to cause damage to the rock due to higher kinetic energy (Fig. 12b); however, as the notches grow the probability of larger rocks getting into the notches decreases. Therefore, the volumetric strain was adjusted based on the notch width to account for the lower probability of larger rocks getting into the notches. In other words, for smaller rock blocks to scour the damaged rocks, the degree of damage must be larger, reflected by larger volumetric strains. Fig. 12c presents the ranges of volumetric strain applied at decreasing widths in the notches and the sizes of broken rocks with respect to the notch geometry.

Based on observations in the field, when slashing occurred, there was a rapid growth at the tips of the notches with slower growth occurring in the walls behind. The damaged rocks in a post-peak state, particularly at the tips of the notches, are highly susceptible to dislodgement under scouring, occurring when falling materials impact the damaged rocks. However, the rock lagging behind the notches along the walls is less

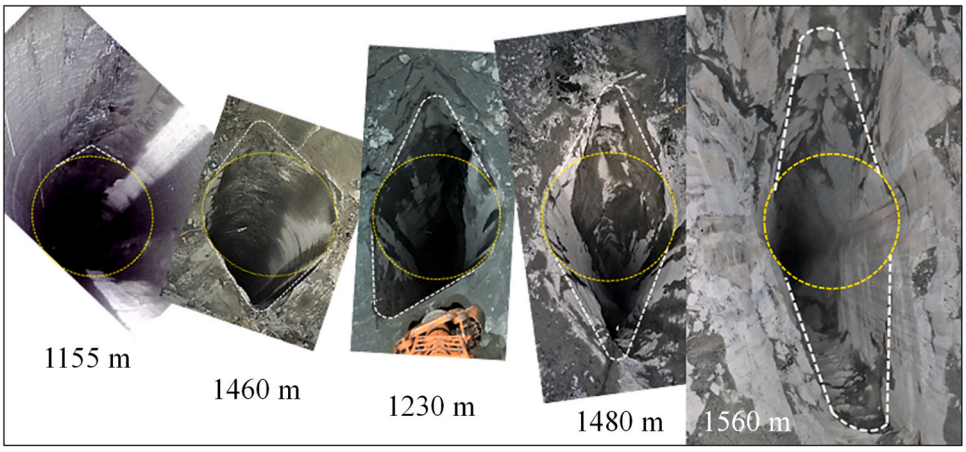

Fig. 11. Images from the Onaping Depth raises showing progressive notch growth at different depths. Note: photos are rotated so that North is up in all images.

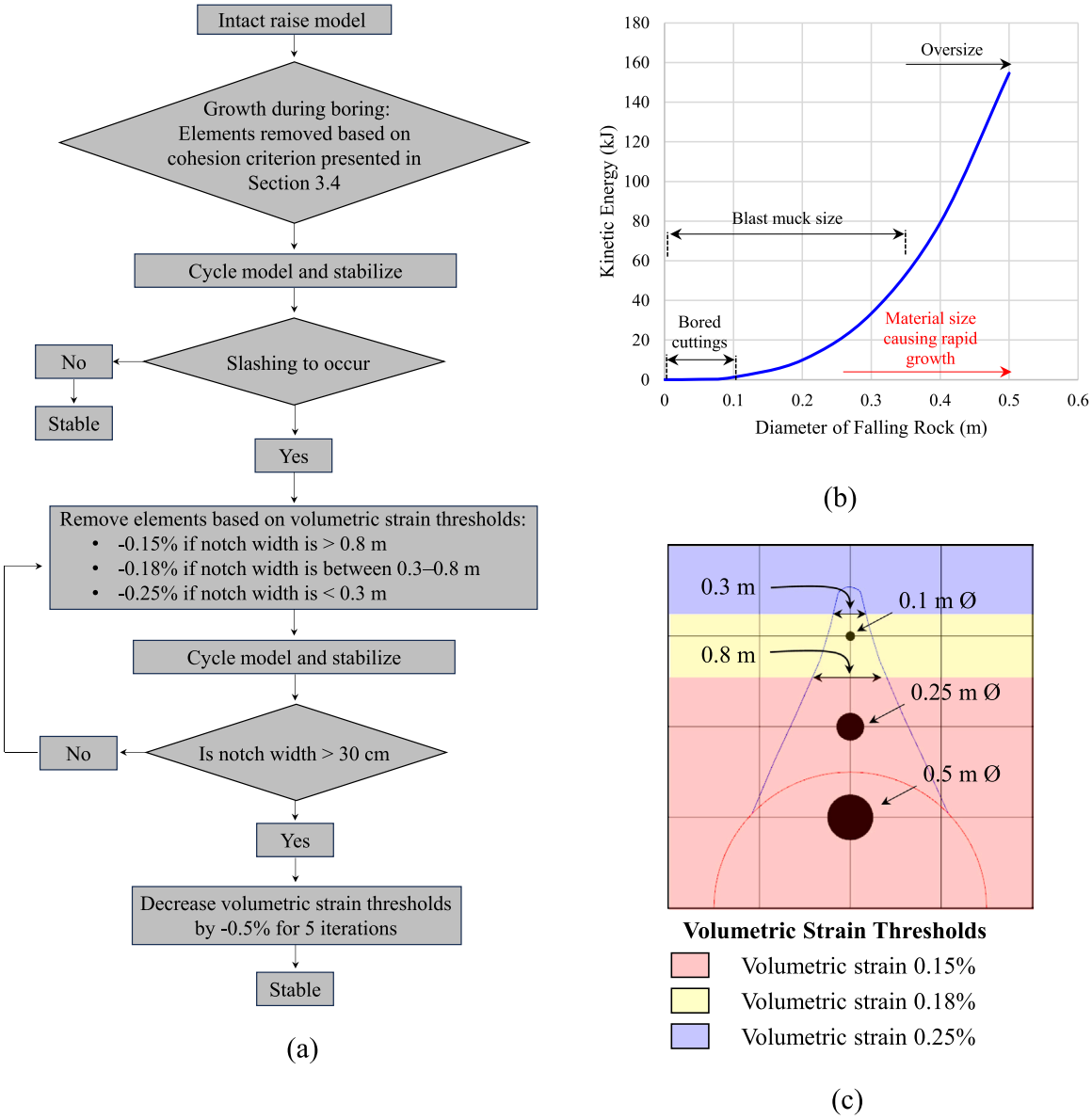

Fig. 12. (a) Flow chart of the methodology for accounting the scouring effect by removing elements meeting criteria in the raise model, (b) the distribution of kinetic energy based on particle size, and (c) the volumetric strain adjustment based on the width of the notch.

susceptible to dislodgement. This is because it has not gone through the same intense stress cycle or experienced the large plastic strains at the notch tips. It is important to note that yielding of rock will not necessarily lead to wall failure, especially if confinement is high or the experienced plastic strain is low. It has also been observed that rock surrounding an excavation can retain cohesive strength even after reaching yield conditions, preventing it from unraveling under gravity loading [33].

The behavior of a rock at the field scale after its peak strength is reached is different from that in the laboratory scale. At the laboratory scale under an unconfined condition, failure in the rock is complete. However, at the field scale, the rock may not exhibit the same level of damage due to boundary constraint and rock confinement. In the notches, the rock exhibits intense fracturing because of the high stresses present in this area – this rock will likely have a significant cohesion and frictional strength loss. However, the walls behind the notches may only exhibit minor fracturing over a much wider area and may not have a complete cohesion and frictional strength loss. Fig. 13a presents the raise model at a late stage of notch growth with elements that have experienced cohesion loss. The cohesion loss threshold is not suitable as the only parameter for element removal because growth will only manifest at the tips of the notches, leading to an elongated narrow geometry that does not agree with field observations. A different parameter, i.e., volumetric strain (Fig. 13b), should be considered for element removal if the simulated notch growth is to match what was observed in the field. Fig. 14 presents various views of the raise at different depths and highlights the higher levels of damage deep in the notches, compared with limited damage sustained to the walls behind the notches.

Volumetric strain, which is defined as the change in volume divided by the original volume, is a parameter that can be tracked in FLAC3D. The evolutionary process of damage in rock has been studied extensively in laboratory testing and several thresholds based on strain changes have been identified [18,50,69,70]. The crack initiation stress correlates with the point for crack initiation. This occurs at 0.3–0.5 times of the peak strength [7,9,34] and can be determined by the deflection point in the deviatoric stress–volumetric strain curve [44]. The onset of fracture coalescence or crack damage stress, which corresponds to the reversal point in the volumetric strain curve, occurs at 0.7–0.8 times of the peak strength [45,50]. A stress–strain curve for a norite sample collected from the Onaping Depth Mine is presented in Fig. 15 with the crack initiation and crack damage thresholds marked.

As rock damage accumulates, the volumetric strain increases until the crack damage threshold is reached, showing a reduction in the sample size. However, as fracture coalescence occurs, the trend reverses and the volume of the sample rapidly increases in the post-peak region as the sample loses integrity. Negative volumetric strain increment indicates rock dilation.

The dilation of the rock mass post-peak is an important factor in the evolution of the notches, as it provides exposure of the yielded material on the walls to direct impact from free-fall materials. This dilated rock mass has little intrinsic strength but good interlock with adjacent material. Using a continuum model, it is not possible to explicitly replicate this failure process. Through a series of tests involving various combinations of model parameters, the volumetric strain was identified as a criterion for replicating the emergent behavior of notch growth observed in the field, which isolated a greater number of elements at the notch tips and fewer along the walls behind the notches.

After a comprehensive trial-and-error investigation related to the 1340 elevation stress conditions, it was found that an initial volumetric strain threshold of −0.15 % for element removal gave the best fit to the field observations. The volumetric strain was reduced further away from the original raise geometry as the notches narrowed to account for the decreasing potential damage that could occur from larger falling rocks. As the notches deepened and narrowed, the probability of larger rocks with higher kinetic energy reaching the notch tips and causing meaningful damage decreases. Therefore, when the notch tip geometry was reduced to 0.8 m wide, the volumetric strain threshold for element removal was decreased to −0.18 %. When the notch geometry was reduced to 0.3 m wide, the volumetric strain threshold was decreased to −0.25 %, which slows the overall growth of the notches.

4. Results

As the notch growth simulation occurs, there are more elements isolated for removal at the notch tips whose volumetric strain was larger than the threshold. Behind the notch tips the elements flagged for removal are more sporadic and not a uniform band. As elements are isolated and then removed from the model, the model is cycled until a stable state is reached. Once the stable state is reached, the element isolation routine is repeated, and the next set of elements are removed if the conditions are met. It is important that the model is stabilized after each iteration because when slashing was paused in the field, the raises were stable with no seismicity or material spalling or sloughing from the walls. The iterative methodology for element stabilization and subsequent removal results in progressive failure of thin bands of elements at the notch tips and irregular element removal along the walls behind the notches. This approach follows field observation while maintaining

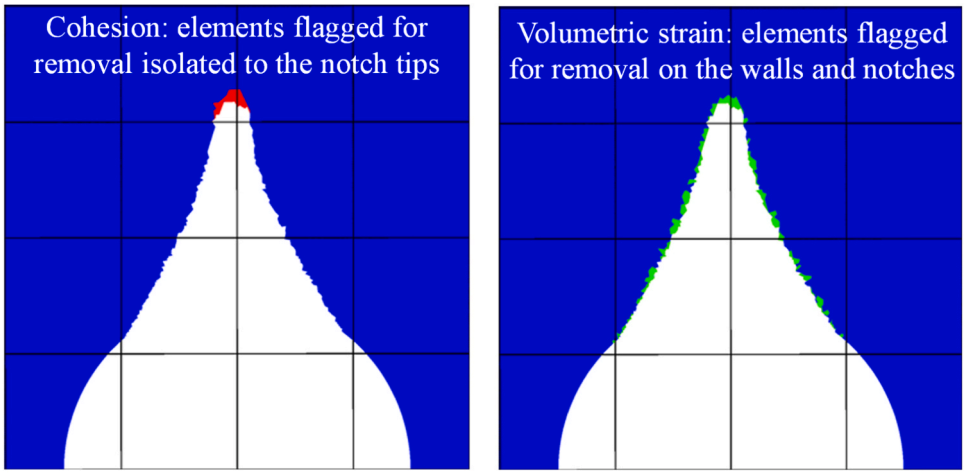

Fig. 13. (a) Elements isolated that have experienced cohesion loss (red) and (b) elements that have reached a volumetric strain of −0.15 % (green).

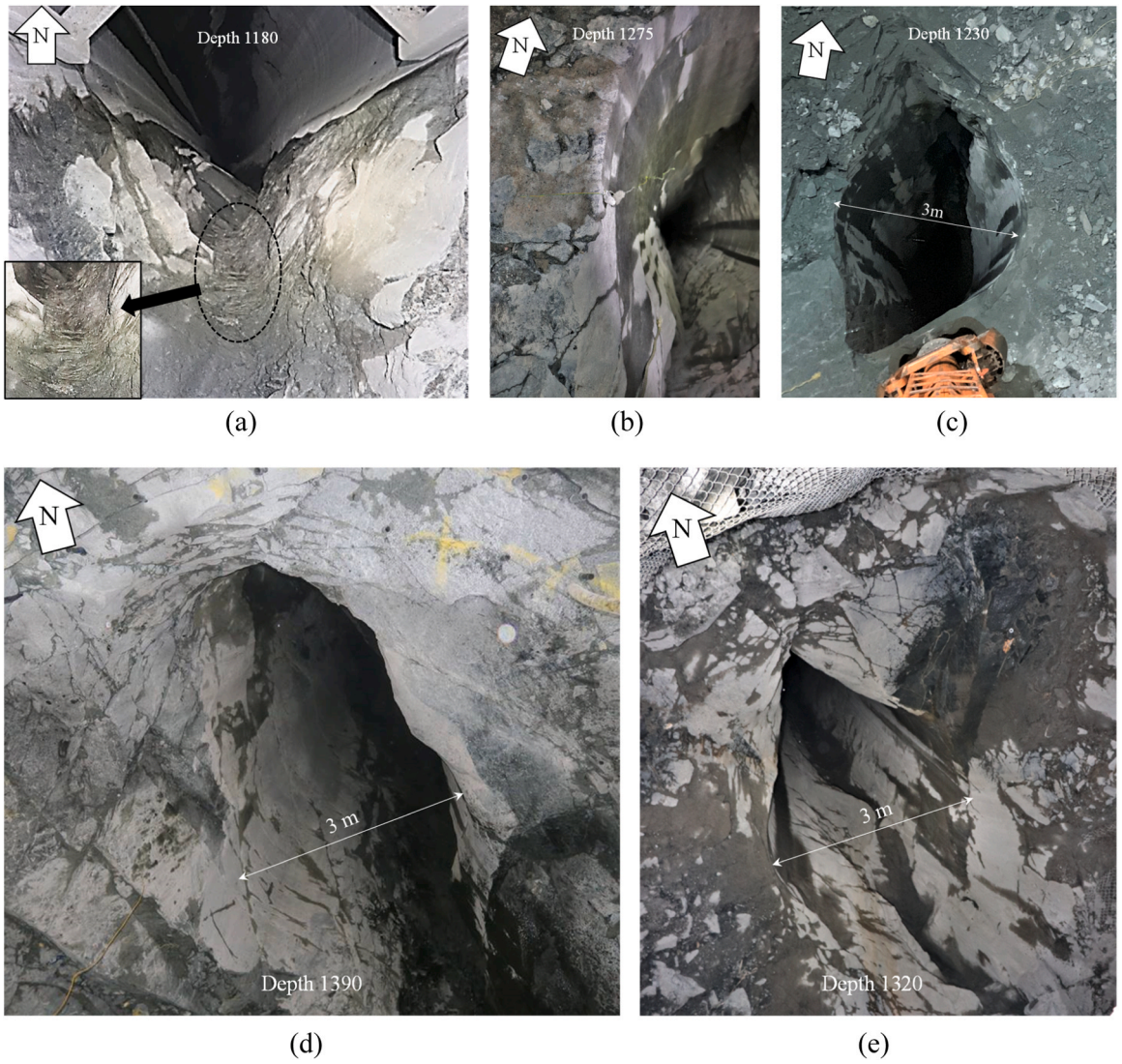

Fig. 14. Various views of the raise while slashing: (a) heavy stress fracturing on the South wall; (b) no stress fracturing observed on the West wall; (c) low to moderate stress fracturing extending into the North wall; (d) tight stress fracturing in the apex of the notch dissipating with increased depth; (e) overall fracturing around the raise.

numerical stability throughout the simulation process.

A series of history points along and adjacent to the path of notch growth was included in the model to track the stress and volumetric strain as the model cycled. Fig. 16 shows the deviatoric stress–volumetric strain relations of two history points in the model as the model simulation progresses. The expected trend is observed with an initial compression of the element as the load increases, followed by a reversal as the stresses reach fracture initiation and peak strength. As the element passes the post-peak region, the element transits from compression into dilation as the load carrying capacity is lost under ongoing strain. The history point positioned at the notch tip experienced a significant increase in deviatoric stress after the peak strength was reached. The history point on the wall of the raise was subject to a lower peak loading cycle, which reduced the likelihood of yielding. However, it was still subject to elastic deformation as the walls reacted to the notch growth.

Due to the significant fracturing on the leading edges (notch tips), elements located in the notches of the raise are more susceptible to scouring failure from material impact compared with the elements located in the walls lagging the notches but the probability of falling rocks impacting the narrow notch tips is low. The reverse is true for the probability of impact on the walls behind the notches; however, the walls have much higher post-peak strength and ability to sustain repeated impacts from falling rocks. Fig. 17 is a conceptual model of the process in which the material most sensitive to impact is the least likely to experience it, while the material most capable of withstanding an impact is far more likely to encounter such events.

As the model simulation progresses and the notch width narrows to 0.8 m, the volumetric strain threshold for element removal is decreased to −0.18 % from −0.15 %. This decrease in volumetric strain threshold leads to slowing of notch growth and further narrowing of the notch. Elements within the wider area of the notches (wider than 0.8 m) are still subject to the lower volumetric strain criteria for removal but there are less elements removed because notch tip, where there is the largest volumetric strain change, has migrated deeper, past this area.

Although there is a reduction in the rate of notch growth, the notches will continue to grow slowly even as the notch tips have tapered. This is a limitation of using a continuum code where scouring is not directly simulated. In the model, elements in the tips of the notches will continue to have larger volumetric strain change and meet the criteria for removal. However, in the field, there is less potential for larger falling rocks to reach the tips of the notches and scour away the stress-damaged rock in the notch tips. Therefore, there must be user discretion for when to stop or slow the model from further notch growth, which is equivalent to no falling rocks impacting the damaged rocks in the notches. Based on

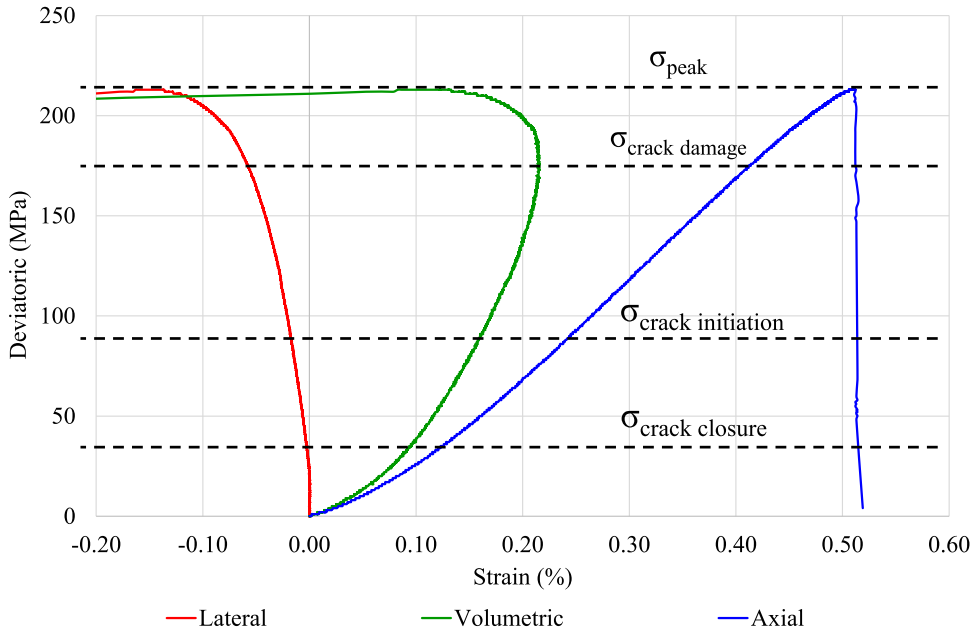

Fig. 15. Stress–strain curves for norite showing characteristic stress thresholds.

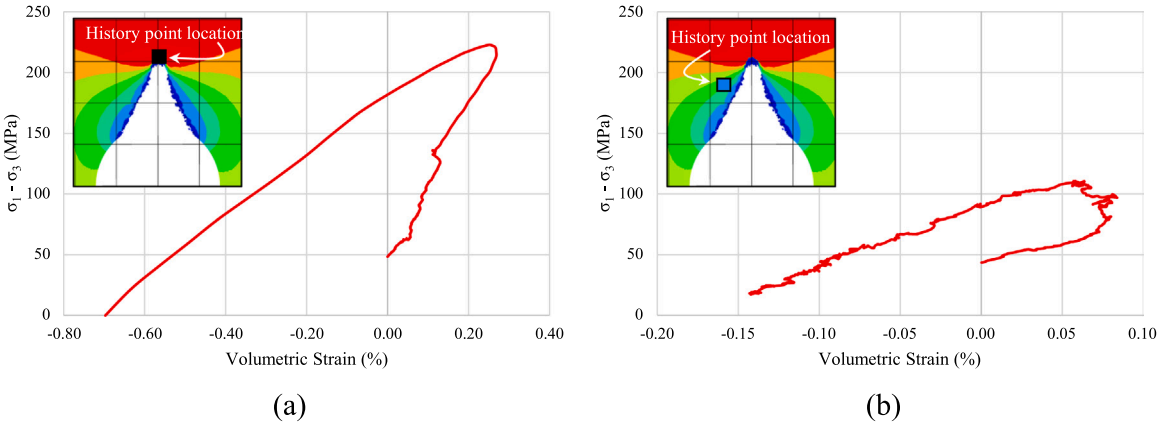

Fig. 16. Evolutions of volumetric strain (a) along the path of the notch growth (shown by a black marker) and (b) offset from the notch tip (shown by the blue marker).

observations, it was our opinion that the main factor limiting further growth was falling rocks' inability to reach the tips of the notches. Falling rocks of increased size will have a larger impact kinetic energy to knock out the stress-damaged rocks at the notch tips. Therefore, for the model simulation, the raise is assumed stable and the threshold for volumetric strain removal is decreased by −0.5 % for five iterations when the width of the notch tips is less than 30 cm, which arrests the notch growth.

Fig. 18 presents a series of plots of cohesive strength, volumetric strain and deviatoric stress from the raise model simulation at 1340 m at various stages of notch growth. Based on the proposed criteria (Fig. 12a), the iterative process was repeated 30 times in this simulation at this depth until the model was stopped. As the iterative process repeats, especially towards the end of the simulation, there are fewer zones removed in each iteration. This slows down the notch growth as the notches elongate and narrow, which was also observed in the field.

As can be seen in Fig. 18a, the cohesion strength criterion initially influences a wider area of the raise, but as the notches elongate, the notch tips become the focal point. The volumetric strain criterion (Fig. 18b) does not have an impact initially; however, as the notch geometry changes, more elements, at the notch tip and a thin layer of elements along the walls lagging behind the notches, meet the removal criterion at the notch tips. Fig. 18c shows that the deviatoric stress at the notch tips are getting higher as the model progresses. It should be noted that at the end of the model iteration, the deviatoric stresses isolated to the notch tips are greater than 200 MPa, which is possible due to the high confinement present at the notch tips.

One of the main purposes of this research was to use the continuum model as a predictive tool to simulate rock mass deformation along the length of the 1150–1440 raise. To test the model as a predictive tool, the same grid detailed above was rerun with the stress conditions expected at 1240, 1440, and 1915 m. The same methodology and criteria were used for removing elements to simulate the notch growth. However, the number of iterations varied for the notch to narrow to the critical width depending on the depth. The models required 36, 30, 27, and 19 iterations for the 1240, 1340, 1440, and 1915 elevations, respectively. The results for the damage sustained during boring using the cohesion removal criterion and the end state after slashing using the volumetric strain criterion are presented in Fig. 19. Overall, the simulated geometries at the other three elevations are similar to that of the 1340 model, but the notch depth increases with the increase of depth. It is seen that the model was successful in replicating the geometry of the raise at

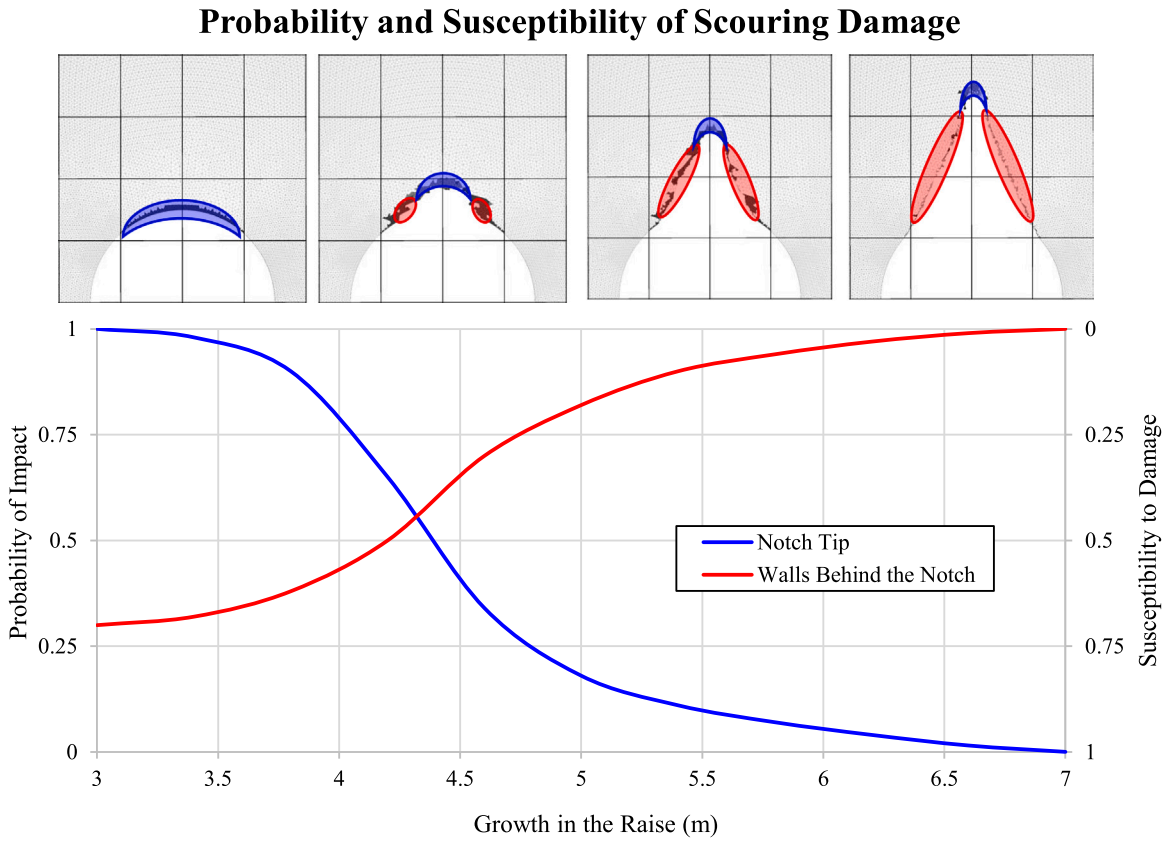

Fig. 17. Conceptual model for the probability of impact and susceptibility to damage of a zone subject to impact forces for the notch tip and notch walls.

increased depth.

The evolution of stress is an important factor in the notch growth in bored raises excavated in brittle rock. Using the same rock strength properties, a FLAC3D model that pre-defines the end state of the raise at the 1340 m level was run and the results are presented in Fig. 20. There is a large divergence between the imposed final geometry and the incremental notch growth process captured in this work. The proposed methodology of progressive element removal to simulate notch growth explicitly in the raises yield a different stress distribution in the final state compared with the results of the simulation that assumes a predefined geometry. This divergence arises due to the path-dependent nature of the notch growth process. Therefore, to achieve a better understanding of bored raise behavior through numerical modeling, it is essential to incorporate progressive growth mechanisms rather than artificially defining the initial and final states of the excavations.

5. Discussions

Using the FLAC3D numerical modeling software, notch growth in the raise was simulated whereby elements that met a set of criteria suitable for fracture formation and scouring were removed. Based on observations made throughout construction of the Onaping Depth winze, it is seen that there was a thin band of stress-fractured rock with the fractures running tangential to the excavation. As these stress-induced fractures were removed with scouring, more stress fractures developed. The objective of the model was to replicate the damage observed in the field and remove these damaged elements in an iterative process. The model was tested at 1240, 1340, 1440 and 1915 elevations and was successful in simulating the notch growth observed in the field. As depth increases, the stresses are higher, resulting in wider and deeper stress fracture zones in the raise. Due to the wider fracture zones, the depth of the notch increases slightly with the overburden. However, notch growth in the raise can arrest if the zone removal is slowed when the notches narrow to less than 20 cm wide.

An important finding, which was observed in the raise and replicated in the model, is that a thin band of stress-fractured rocks in the walls of the raise promotes stability. In the field, the raise excavation remained stable as long as the thin band of stress-fractured rocks remained in place. The damaged rocks provide confinement, which suppresses spalling, strainbursting, and associated seismicity. However, when the rocks are removed, the system becomes unstable, resulting in the aforementioned activity and generation of more stress fractures to restabilize the excavation. The importance of the fractured rocks for notch stabilization was also replicated in the model. When the fractured rocks are removed, the model generates additional damage, which in turn stabilizes the model and limits damage.

The main limitation of the approach used in this study is related to the inability of FLAC3D to simulate fracturing directly. The iterative element removal approach presented in this study can also be applied to discontinuum modeling methods for more accurate simulation of notch growth in bored raises. The model does not account for variability in rock strength nor considers geological structures, which can lead to different notch geometric profiles. These aspects can be explored in further work. Although not completed in this work, this modeling methodology can also be applied to inclined waste passes at the Onaping Depth Mine where scouring will damage walls that do not exhibit stress-induced damage. In this case, any damage sustained to the East or West walls will result in increased notch depth because any increase in span will result in extended iterations of zone removal prior to the notch narrowing to a critical width.

Although this study focused on the walls of the raise, further effort should be taken to examine the rock mass response at the face where the bore is grinding the rock. While pulling raises at Onaping Depth, numerous failures of the cutters on the bore resulted in significant delays due to the need for repairs. Ground squeezing in a plastic manner is not possible in the stiff rock masses at Onaping Depth. However, dilation of

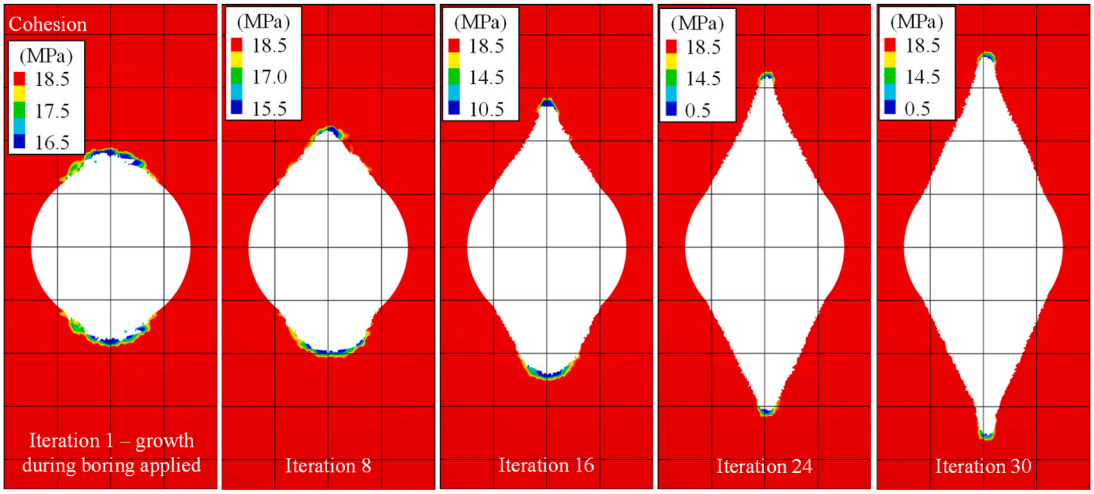

(a)

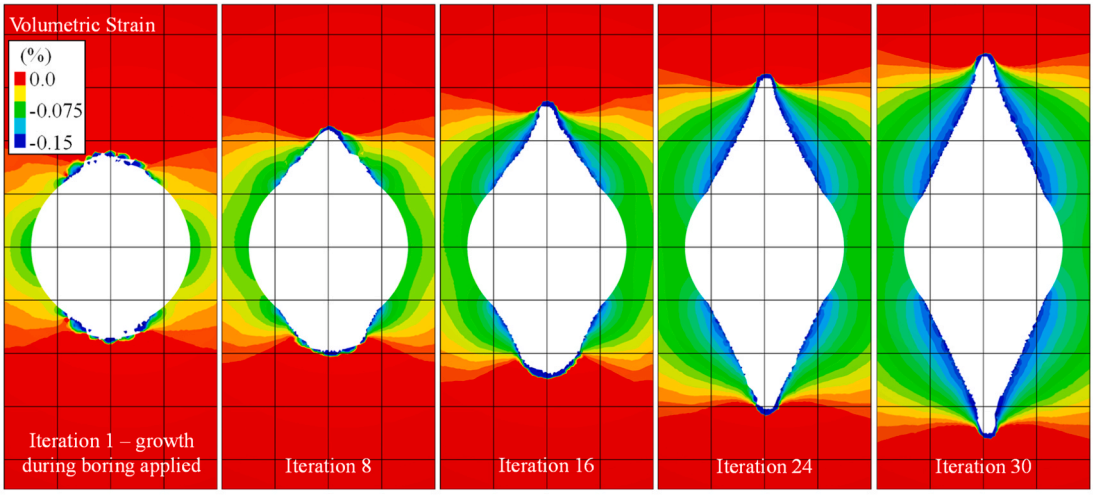

(b)

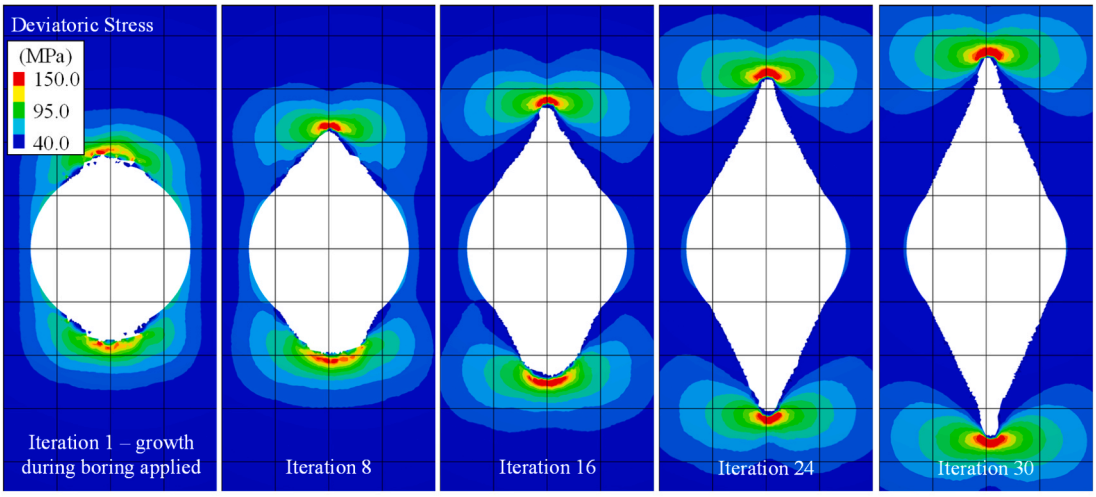

(c)

Fig. 18. Simulation of the notch growth at 1340 m depth: (a) plots of cohesion strength as the notches grow, (b) plots of volumetric strain, and (c) plots of deviatoric stress as the notches grow. Note: 1 m × 1 m squares are overlaid on all plots for scale.

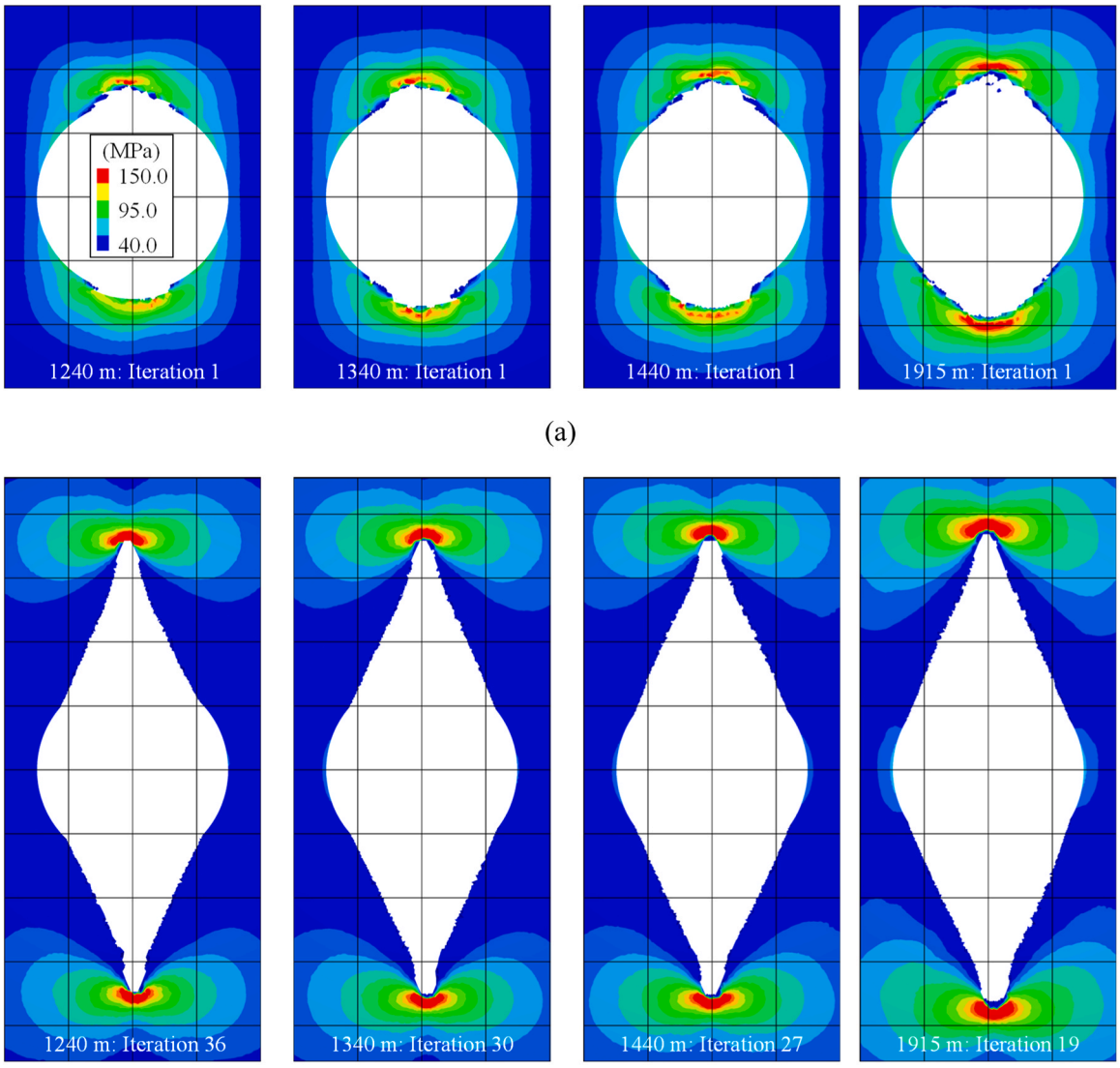

Fig. 19. Simulation of notch growth at 1240, 1340, 1440, and 1915 m using (a) the cohesion loss criterion and (b) the volumetric strain criterion with contours of deviatoric stress.

the stress-fractured rock on the North and South sides of the raise could clamp the bore in place. For this reason, the contractor was instructed to maintain continuous rotation of the bore and to keep it as close to the face as possible, where there is less dilation due to the high levels of confinement at the corners.

It was found through several LiDAR scans that the vertical face was dishing as stress-fractured rocks spalled off. Therefore, instead of all cutters being in contact with the rock at the face, evenly distributing the load of pulling on all the cutters, only the outside cutters were taking the load, resulting in excess wear and failure of these cutters specifically. Simulation of this phenomenon could facilitate a review of bore designs used in highly stressed brittle rocks.

The lessons learned from this study are beneficial for raises to be driven in brittle rock in high horizontal stress environments at depth. It is recommended that mines that are considering excavating raises in deep mines collect as much data as possible to understand the rock mass conditions and in-situ stresses to make informed engineering decisions for safe construction of the raises. Although the simulation based on the damage criterion described in this research matched the notch growth observed in the Onaping Depth raises, the criterion must be calibrated to the conditions encountered at other mine sites. In addition, the iterative approach of removing thin bands elements should be applied to observe the emergent behavior of notch growth in bored excavations.

6. Conclusion

This study details the simulation of notch growth in two 3 m diameter raises excavated in brittle rock. The purpose of this work is to replicate the notch growth observed in the raises, enabling better predictions of bored raise stability, particularly in cases where existing empirical methods and numerical modeling approaches may inadequately capture the depth of failure resulting from the removal of stress-fractured rocks along critically stressed raise walls.

A FLAC3D model was constructed and calibrated using laboratory testing and field observation data gathered throughout the shaft excavation. Due to the limitations of FDM codes to simulate fracturing directly, a damage criterion considering cohesion and volumetric strain was developed. The cohesion loss criterion was used to simulate damage

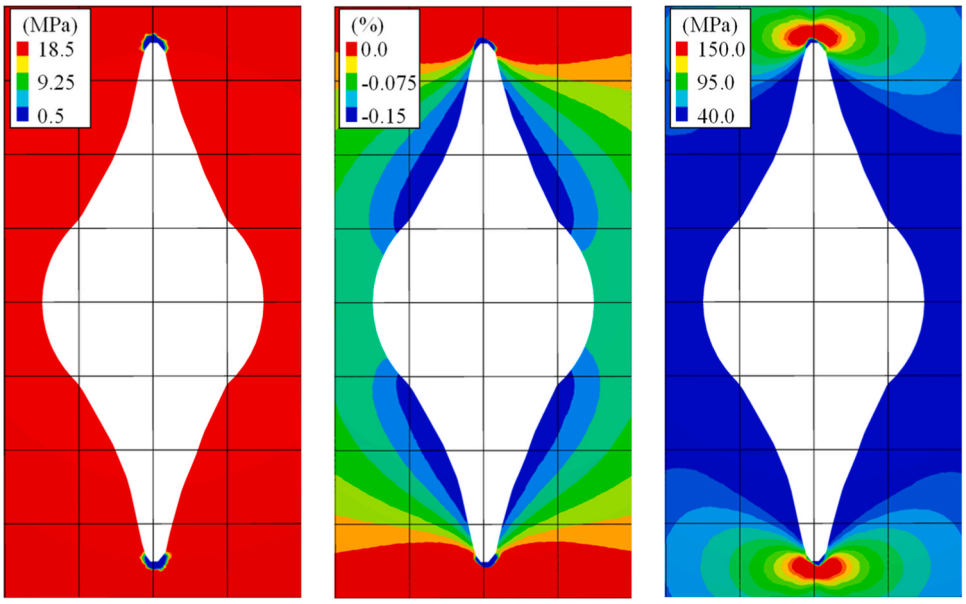

Fig. 20. Plots of a model simulation at 1440 m without progressive notch growth: (a) cohesion strength, (b) volumetric strain, and (d) deviatoric stress.

sustained to the excavation during the boring process and subsequent scouring from small, bored cuttings; the volumetric strain criterion was used to simulate scouring from larger rocks during slashing by drill-and-blasting. When elements meet the criteria, they are removed from the model, and the model is cycled to equilibrium. As the model stabilizes, some elements may meet the criteria, qualifying for removal. The model can eventually stabilize because when scouring is stopped, the excavations stabilize, and further deterioration stops.

Through this iterative process of removing elements and allowing additional damage to occur, the emergent behavior of gradual notch formation is captured. The depth of failure, represented by the actual notches formed, is different from the conventional approach of using yielding elements to represent the failure zones in continuum models. The simulation results of the notch growth agree well with field observation, demonstrating the feasibility of the proposed approach. This seems to be the first time that the scouring effect is considered in a continuum numerical model. Being able to simulate notch growth considering all possible influence factors can assist us in developing a strategy for proactively mitigating risks associated with the construction of bored raises and shafts.

CRediT authorship contribution statement

Alex Hall: Writing – original draft. **Ming Cai:** Supervision. **Chris O'Connor:** Project administration. **Brad Simser:** Writing – review & editing. **Pranay Yadav:** Project administration, Conceptualization.

Declaration of Competing Interest

The authors declare that they have no known competing financial interests or personal relationships that could have appeared to influence the work reported in this paper. Ming Cai is associate editor and did not participate in the review process.

Acknowledgments

The authors would like to thank the Glencore Sudbury Integrated Nickel Operations management team for allowing the publication of this paper.

References

[1] M.S. Abdollahi, M. Najafi, A.Y. Bafghi, M.F. Marji, A 3D numerical model to determine suitable reinforcement strategies for passing TBM through a fault zone, a case study: Safaroud water transmission tunnel, Iran, Tunn. Undergr. Space Technol. 88 (2019) 186–199, https://doi.org/10.1016/j.tust.2019.03.008.
[2] J.C. Andersson, C.D. Martin, H. Stille, The Äspö pillar stability experiment: part II—rock mass response to coupled excavation-induced and thermal-induced stresses, Int. J. Rock. Mech. Min. Sci. 46 (2009) 879–895.
[3] B. Arjang, G. Herget, In situ ground stresses in the Canadian hardrock mines: An update, Int. J. Rock. Mech. Min. Sci. 34 (1997) 15.e1–15.e16, https://doi.org/10.1016/S1365-1609(97)00039-7.
[4] G. Bäckblom, C.D. Martin, Recent experiments in hard rocks to study the excavation response: Implications for the performance of a nuclear waste geological repository, Tunn. Undergr. Space Technol. 14 (1999) 377–394, https://doi.org/10.1016/S0886-7798(99)00053-X.
[5] P.-E. Bernard, J.-F. Remacle, N. Kowalski, C. Geuzaine, Frame field smoothness-based approach for hex-dominant meshing, Comput. -Aided Des. 72 (2016) 78–86.
[6] Z.T. Bieniawski, Engineering rock mass classifications: a complete manual for engineers and geologists in mining, civil, and petroleum engineering, John Wiley & Sons, 1989.
[7] Z.T. Bieniawski, Mechanism of brittle fracture of rock: part I—theory of the fracture process, in: International Journal of Rock Mechanics and Mining Sciences & Geomechanics Abstracts, Elsevier, 1967, pp. 395–406.
[8] M. Board, Examination of the use of continuum versus discontinuum models for design and performance assessment for the Yucca Mountain site, Nucl. Regul. Comm. (1989).
[9] W.F. Brace, B.W. Paulding Jr, C.H. Scholz, Dilatancy in the fracture of crystalline rocks, J. Geophys. Res. 71 (1966) 3939–3953.
[10] M. Cai, Influence of stress path on tunnel excavation response – Numerical tool selection and modeling strategy, Tunn. Undergr. Space Technol. 23 (2008) 618–628, https://doi.org/10.1016/j.tust.2007.11.005.
[11] M. Cai, P.Y. Hou, X.W. Zhang, X.T. Feng, Post-peak stress–strain curves of brittle hard rocks under axial-strain-controlled loading, Int. J. Rock. Mech. Min. Sci. 147 (2021) 104921.
[12] M. Cai, P.K. Kaiser, In-situ rock spalling strength near excavation boundaries, Rock. Mech. Rock. Eng. 47 (2014) 659–675.
[13] M. Cai, P.K. Kaiser, Y. Tasaka, T. Maejima, H. Morioka, M. Minami, Generalized crack initiation and crack damage stress thresholds of brittle rock masses near underground excavations, Int. J. Rock. Mech. Min. Sci. 41 (2004) 833–847.
[14] Ø. Dammyr, Prediction of Brittle Failure for TBM Tunnels in Anisotropic Rock: A Case Study from Northern Norway, Rock. Mech. Rock. Eng. 49 (2016) 2131–2153, https://doi.org/10.1007/s00603-015-0910-z.
[15] M.S. Diederichs, The 2003 Canadian Geotechnical Colloquium: Mechanistic interpretation and practical application of damage and spalling prediction criteria for deep tunnelling, Can. Geotech. J. 44 (2007) 1082–1116.
[16] M.S. Diederichs, T. Carter, C.D. Martin, Practical rock spall prediction in tunnels, in: Proceedings of ITA World Tunnel Congress, 2010, p. 1e8.
[17] M.S. Diederichs, P.K. Kaiser, E. Eberhardt, Damage initiation and propagation in hard rock during tunnelling and the influence of near-face stress rotation, Int. J.

Rock. Mech. Min. Sci. 41 (2004) 785–812, https://doi.org/10.1016/j.ijrmms.2004.02.003.
[18] E. Eberhardt, D. Stead, B. Stimpson, R.S. Read, Identifying crack initiation and propagation thresholds in brittle rock, Can. Geotech. J. 35 (1998) 222–233.
[19] Emsley, S., Olsson, O., Stenberg, L., Alheid, H.-J., Falls, S., 1997. ZEDEX-A study of damage and disturbance from tunnel excavation by blasting and tunnel boring.
[20] Y. Fan, W. Lu, Y. Zhou, P. Yan, Z. Leng, M. Chen, Influence of tunneling methods on the strainburst characteristics during the excavation of deep rock masses, Eng. Geol. 201 (2016) 85–95, https://doi.org/10.1016/j.enggeo.2015.12.015.
[21] Q.M. Gong, L.J. Yin, S.Y. Wu, J. Zhao, Y. Ting, Rock burst and slabbing failure and its influence on TBM excavation at headrace tunnels in Jinping II hydropower station, Eng. Geol. 124 (2012) 98–108, https://doi.org/10.1016/j.enggeo.2011.10.007.
[22] H.-X. Guo, X. Liu, D.-M. Yan, Y. Liu, Cut-enhanced PolyCube-maps for feature-aware all-hex meshing, ACM Trans. Graph. TOG 106 (39) (2020) 1–106, 14.
[23] V. Hajiabdolmajid, P. Kaiser, C.D. Martin, Mobilised strength components in brittle failure of rock, Geotechnique 53 (2003) 327–336.
[24] V. Hajiabdolmajid, P.K. Kaiser, C.D. Martin, Modelling brittle failure of rock, Int. J. Rock. Mech. Min. Sci. 39 (2002) 731–741, https://doi.org/10.1016/S1365-1609(02)00051-5.
[25] A. Hall, M. Cai, B. Simser, J. Lindsay, Notch formation in vertical excavations in a deep hard rock mine and rock stabilization methodologies, Deep Resour. Eng. 1 (2024) 100003, https://doi.org/10.1016/j.deepre.2024.100003.
[26] A. Hall, B. Simser, M. Cai, Mechanisms of deterioration in a bored raise in brittle rock, Int. J. Rock. Mech. Min. Sci. 139 (2021) 104666.
[27] R. Hasanpour, J. Schmitt, Y. Ozcelik, J. Rostami, Examining the effect of adverse geological conditions on jamming of a single shielded TBM in Uluabat tunnel using numerical modeling, J. Rock. Mech. Geotech. Eng. 9 (2017) 1112–1122, https://doi.org/10.1016/j.jrmge.2017.05.010.
[28] S. Heidarzadeh, A. Saeidi, A. Rouleau, The damage-failure criteria for numerical stability analysis of underground excavations: A review, Tunn. Undergr. Space Technol. 107 (2021) 103633, https://doi.org/10.1016/j.tust.2020.103633.
[29] F.E. Heuze, Scale effects in the determination of rock mass strength and deformability, Rock. Mech. 12 (1980) 167–192.
[30] Hoek, E., 2023. Practical Rock Engineering.
[31] E. Hoek, E.T. Brown, The Hoek–Brown failure criterion and GSI – 2018 edition, J. Rock. Mech. Geotech. Eng. 11 (2019) 445–463, https://doi.org/10.1016/j.jrmge.2018.08.001.
[32] Hoek, E., Carranza-Torres, C., Corkum, B., Hoek, Evert, Carranza-Torres, Carlos, 2002. Hoek-Brown failure criterion - 2002 Edition.
[33] E. Hoke, E.T. Brown, Underground excavation in rock, Inst. Min. Met. (1980).
[34] D.J. Holcomb, L.S. Costin, Damage in brittle materials: experimental methods. Sandia National Labs., Albuquerque, NM (USA). Geomech. Div. (1986).
[35] H. Huang, J. Shen, Q. Chen, M. Karakus, Estimation of REV for fractured rock masses based on Geological Strength Index, Int. J. Rock. Mech. Min. Sci. 126 (2020) 104179.
[36] W.A. Hustrulid, W.A. Hustrulid, R.C. Bullock, R.L. Bullock, Underground mining methods: Engineering fundamentals and international case studies, SME (2001).
[37] Itasca, 2023a. FLAC3D. Itasca Consulting Group, Inc., Minneapolis, MN, USA.
[38] Itasca, 2023b. Griddle. Itasca Consulting Group, Inc., Minneapolis, MN, USA.
[39] L. Jing, A review of techniques, advances and outstanding issues in numerical modelling for rock mechanics and rock engineering, Int. J. Rock. Mech. Min. Sci. 40 (2003) 283–353, https://doi.org/10.1016/S1365-1609(03)00013-3.
[40] Kaiser, P.K., 2019. From common to best practices in underground rock engineering, in: ISRM Congress. ISRM, p. ISRM-14CONGRESS-2019-008.
[41] P.K. Kaiser, M.S. Diederichs, C.D. Martin, J. Sharp, W. Steiner, Underground works in hard rock tunnelling and mining, in: ISRM International Symposium, ISRM, 2000 p. ISRM-IS-2000-021.
[42] P.K. Kaiser, S. Maloney, Review of ground stress database for the Canadian Shield, Ont. Power Gener. (2005).
[43] P.K. Kaiser, D.R. McCreath, Rock mechanics considerations for drilled or bored excavations in hard rock, Tunn. Undergr. Space Technol. 9 (1994) 425–437, https://doi.org/10.1016/0886-7798(94)90101-5.
[44] H. Li, R. Zhong, L. Pel, D. Smeulders, Z. You, A New Volumetric Strain-Based Method for Determining the Crack Initiation Threshold of Rocks Under Compression, Rock. Mech. Rock. Eng. 57 (2024) 1329–1351, https://doi.org/10.1007/s00603-023-03619-2.
[45] D.A. Lockner, J.D. Byerlee, V. Kuksenko, A. Ponomarev, A. Sidorin, Observations of quasistatic fault growth from acoustic emissions. International Geophysics, Elsevier, 1992, pp. 3–31.
[46] J.C. Long, J.S. Remer, C.R. Wilson, P.A. Witherspoon, Porous media equivalents for networks of discontinuous fractures, Water Resour. Res. 18 (1982) 645–658.
[47] M. Lyon, D. Bommes, L. Kobbelt, HexEx: Robust hexahedral mesh extraction, ACM Trans. Graph. TOG 35 (2016) 1–11.
[48] C.D. Martin, Seventeenth Canadian Geotechnical Colloquium: The effect of cohesion loss and stress path on brittle rock strength, Can. Geotech. J. 34 (1997) 698–725, https://doi.org/10.1139/t97-030.
[49] C.D. Martin, The strength of massive Lac du Bonnet granite around underground openings (Ph. D. thesis), University of Manitoba., Winnipeg, Canada, 1993.
[50] C.D. Martin, N.A. Chandler, The progressive fracture of Lac du Bonnet granite, in: International Journal of Rock Mechanics and Mining Sciences & Geomechanics Abstracts, Elsevier, 1994, pp. 643–659.
[51] C.D. Martin, R. Christiansson, Estimating the potential for spalling around a deep nuclear waste repository in crystalline rock, Int. J. Rock. Mech. Min. Sci. 46 (2009) 219–228, https://doi.org/10.1016/j.ijrmms.2008.03.001.
[52] C.D. Martin, R. Christiansson, J. Söderhäll, Rock stability considerations for siting and constructing a KBS-3 repository. Based on experiences from Aespoe HRL, AECL's URL, tunnelling and mining, Swed. Nucl. Fuel Waste Manag. Co. (2001).
[53] C.D. Martin, P.K. Kaiser, D.R. McCreath, Hoek-Brown parameters for predicting the depth of brittle failure around tunnels, Can. Geotech. J. 36 (1999) 136–151.
[54] D. Martin, R.S. Read, AECL's Mine-by experiment: A test tunnel in brittle rock, in: Rock Mechanics Tools and Techniques, 1996, pp. 13–24.
[55] C.D. Martini, R.S. Read, J.B. Martino, Observations of brittle failure around a circular test tunnel, Int. J. Rock. Mech. Min. Sci. 34 (1997) 1065–1073.
[56] K.-B. Min, L. Jing, Numerical determination of the equivalent elastic compliance tensor for fractured rock masses using the distinct element method, Int. J. Rock. Mech. Min. Sci. 40 (2003) 795–816.
[57] Nozari, A., Khosravi, M.H., 2016. numerical study on the effect of mechanical precutting and fiber glass bolts in Alborz tunnel passing through Kandovan fault 5, 99–112.
[58] M. Oda, A method for evaluating the representative elementary volume based on joint survey of rock masses, Can. Geotech. J. 25 (1988) 440–447.
[59] W.G. Pariseau, S. Puri, S.C. Schmelter, A new model for effects of impersistent joint sets on rock slope stability, Int. J. Rock. Mech. Min. Sci. 45 (2008) 122–131.
[60] Read, R.S., Martin, C.D., 1996. Technical summary of AECL's Mine-by Experiment phase I: Excavation response. Canada.
[61] R.A. Schultz, Relative scale and the strength and deformability of rock masses, J. Struct. Geol. 18 (1996) 1139–1149.
[62] S. Song, F. Sun, J. Chen, W. Zhang, X. Han, X. Zhang, Determination of RVE size based on the 3D fracture persistence, Q. J. Eng. Geol. Hydrogeol. 50 (2017) 60–68.
[63] K. Thuro, R.J. Plinninger, Hard Rock Tunnel Boring, Cutting, Drilling And Blasting: Rock Parameters For Excavatability, Presente 10th ISRM Congr. (2003). ISRM-10CONGRESS-2003-212.
[64] I. Vazaios, M.S. Diederichs, N. Vlachopoulos, Assessment of strain bursting in deep tunnelling by using the finite-discrete element method, J. Rock. Mech. Geotech. Eng. 11 (2019) 12–37, https://doi.org/10.1016/j.jrmge.2018.06.007.
[65] X. Wang, Y. Zhao, X. Lin, Determination of mechanical parameters for jointed rock masses, J. Rock. Mech. Geotech. Eng. 3 (2011) 398–406.
[66] Q. Wu, P.H. Kulatilake, REV and its properties on fracture system and mechanical properties, and an orthotropic constitutive model for a jointed rock mass in a dam site in China, Comput. Geotech. 43 (2012) 124–142.
[67] R. Yoshinaka, M. Osada, H. Park, T. Sasaki, K. Sasaki, Practical determination of mechanical design parameters of intact rock considering scale effect, Eng. Geol. 96 (2008) 173–186.
[68] W. Zhang, J. Chen, C. Liu, R. Huang, M. Li, Y. Zhang, Determination of geometrical and structural representative volume elements at the Baihetan dam site, Rock. Mech. Rock. Eng. 45 (2012) 409–419.
[69] X.-P. Zhang, G.-G. Lv, Q.-S. Liu, S.-C. Wu, Q. Zhang, P.-Q. Ji, X.-H. Tang, Identifying accurate crack initiation and propagation thresholds in siliceous siltstone and limestone, Rock. Mech. Rock. Eng. 54 (2021) 973–980.
[70] Z. Zhao, Y. Shou, X. Zhou, Microscopic cracking behaviors of rocks under uniaxial compression with microscopic multiphase heterogeneity by deep learning, Int. J. Min. Sci. Technol. 33 (2023) 411–422.
[71] H. Zhou, Y. Gao, C. Zhang, F. Yang, M. Hu, H. Liu, Y. Jiang, A 3D model of coupled hydro-mechanical simulation of double shield TBM excavation, Tunn. Undergr. Space Technol. 71 (2018) 1–14, https://doi.org/10.1016/j.tust.2017.07.012.

Alex Hall is a PhD candidate in Engineering Science at Laurentian University. The primary focus of his research is on the stability of vertical excavations with specific emphasis on precondition blasting to promote safe working conditions for operators. He has published several scientific papers on this topic. Mr. Hall is currently an Engineering Specialist with Glencore, working of the Onaping Depth Project. Prior to joining Glencore, Mr. Hall worked as a consultant for Itasca on various projects internationally and as an Operations Engineer for PotashCorp and Vale Inco. He holds BSc and MASc in Mining Engineering. His areas of specialization are: deep mining, mine design, mine sequencing, planning, vertical excavations including bored raises and shaft sinking, ground control, and drilling and blasting.

Dr. Cai is a Full Professor in Laurentian University's School of Engineering and Computer Science and holds a position as Geomechanics Research Chair. Dr. Cai holds Bachelor and Master degrees from Tsinghua University in China and a PhD degree from the University of Tokyo in Japan. Prior to joining Laurentian, he worked for Mansour Group Inc., MIRARCO, Tokyo Electric Power Services Ltd., and Tsinghua University and had over 30 years' research, education, and industry experience. He has a wide variety of interests in rock mechanics and rock engineering, and has made exceptional technical and scientific contributions to many topics including constitutive modeling of rock masses, rock mass characterization, rock support in burst-prone ground, interpretation of AE and microseismic monitoring data, and rock failure process simulation. Dr. Cai is the author/co-author of more than 250 scientific publications. He was awarded the Canadian Geotechnical Society's John A. Franklin Award in 2017.